POLITECNICO
MILANO 1863

SCUOLA DI INGEGNERIA INDUSTRIALE
E DELL'INFORMAZIONE

Development and test of models to scale rain attenuation from Ka to EHF bands

Tesi di Laurea Magistrale in
Space Engineering

Author: **Davide Allievi**

Student ID: 970999
Advisor: Prof. Lorenzo Luini
Academic Year: 2022-23

Abstract

This thesis presents a frequency scaling model based on a physical approach from Ka to EHF bands. The scaling is compared with the well known Drufuca scaling method, which it is an empirical one. To improve the physical basis of the method a DSD model is introduced and the α and k coefficients of the rain attenuation are computed. The scaled results are compared with the real rain attenuations at the frequencies of interest (18.7, 39.6 and 49.5 GHz) obtained from the biennial data-set (1995-1996). Data come from a beacon link between the Earth station located in Spino D'Adda (45.4°N, 9.5 °E, altitude 84 m a.m.s.l.) and the geostationary satellite ITALSAT. The scaled results are compared following the error figure presented in ITU-R P.311-18 and the evaluation is made computing the covariance and the mean value of the error between the scaled data and the real data in ccdf form. Results indicate that the physically based frequency scaling approach offers improved results.

Keywords: Frequency scaling, rain attenuation, satellite communications, tropospheric attenuation, EM wave propagation, radiometry

Sommario

In questa tesi è presentato un modello di " frequency scaling" basato su un approccio fisico dalla banda Ka alle bande EHF. La scalatura ottenuta è comparata con il ben noto metodo empirico di Drufuca, il quale è un metodo empirico. Per migliorare la base fisica della scalatura è introdotto un modello di DSD per ottenere i coefficienti α e k presenti nella formulazione dell'attenuazione da pioggia. I risultati della scalatura sono comparati con la attenuazione da pioggia reale alle frequenze di interesse (18.7, 39.6 e 49.5 GHz), ottenute da un dataset biennale (1995-1996). Il dataset proviene dal collegamento tra il beacon presente nella stazione di terra di Spino D'Adda (45.4°N, 9.5 °E, altitude 84 m a.m.s.l.) ed il satellite geostazionari ITALSAT. I risultati ottenuti sono comparati seguendo la "figura d'errore" presentata nella ITU-R P.311-18, la valutazione è compiuta tra i dati scalati e reali in forma ccdf. I risultati ottenuti con il metodo implementato nella tesi offrono dei risultati migliori.

Keywords: Frequency scaling, attenuazione da pioggia, comunicazione satellitare, attenuazione troposferica, propagazione di onde elettromagnetiche, radiometria

Contents

Introduction

In the telecommunication systems between satellites and ground station high frequencies are used. The pro of high frequency is the high amount of data that can be exchanged between the link. The large amount of data is fundamental for complex missions (maintain the attitude, perform a maneuver, do a fly-by...). Another problem of low bands is that they are congested so it is almost mandatory nowadays use always higher frequencies. The frequencies of interest in this thesis are the Ka band (18.7 GHz), the Q band (39.6 GHz) and the V band (49.5 GHz). The link of interest is the one between spacecraft (SC) and ground station (GS). The signal between SC and GS occurs some disturbances due to atmosphere presence, in particular this thesis goes thorough the tropospheric attenuation contribution, characterized by the following effects:

- Gas attenuation, divided into its component: oxygen and water vapour attenuation
- Cloud attenuation
- Rain attenuation
- Scintillation

In the first part of the thesis each component of the total attenuation is indagated at Ka, Q and V band thanks to data provided by beacons, meteorological stations and theoretical models. To do that the following instruments are installed in Spino d'Adda Earth station and used:

- Radiometer, working at 13.00, 23.84 and 31.65 GHz. It is used to derive the integrated liquid water content and the integrated water vapor content. From these data it is possible to retrieve the tropospheric attenuation in non-rainy condition.
- Set of standard meteorological instruments:
  - thermometer
  - hygrometer
  - barometer
  - rain gauge

The downside of the use of high frequency between SC and GC is the lack of attenuation models of the high frequencies, for this reason one of the most common and used approach to cope with this problem is to use frequency scaling. Two possible ways exist to perform frequency scaling: the first one is an empirical approach (where the principal method is Drufuca's one [6]), the second one is a physical approach: the frequency scaling is performed based on the physical formulation of the attenuation of interest.
In the second part of this thesis, it is proposed a frequency scaling model for rain attenuation based on a physical approach and Drufuca's scaling is used as comparison.
As last step the scaled model are evaluated with respect to the data and the goodness of the scaling is assessed computing the mean value (MV) and the root mean square (RMS) of the prediction error.

1 | Attenuation of the signal due to troposperic effects

This chapter studies and presents the tropospheric attenuations that are present on the link between the GS and the SC that are influencing frequencies above 10 GHz.

1.1. Scintillations

The scintillations are a secondary effect which is present as disturb on the signal whose frequency is above 10 GHz. They are a very complex contributions, they are caused by inhomogeneities in the medium, turbulence, variations of temperature and pression, presence of clouds or rain events and wind. This last contribution changes the atmospheric propagation path and it becomes less homogeneous, which causes temporal and spatial variations in the refractive index which in non-windy and non-turbulent conditions would change slowly in horizontal plane and regularly with height. The receiver reads scintillations as a rapid variation in both phase and amplitude fluctuations.
The root mean square value of the monthly fluctuation is correlated with the wet term of the radio refractivity, N_{wet}. It is possible to evaluate N_{wet} thanks to the ITU-R P.453-11 [17] model as:

$$N_{wet} = 72\frac{e}{T} + 3.75 \cdot 10^5 \frac{e}{T^2} \tag{1.1}$$

T is the temperature in K and e is water vapour pressure in hPa

1.2. Gas attenuation

An electromagnetic signal propagating through Earth's atmosphere will be subject to a power reduction due to gas absorption. This attenuation depends on many factors as the frequency of the signal, the link's elevation, the temperature, the pressure and the water vapour concentration.
The Earth's atmosphere composition as dry air contains 78.08% nitrogen, 20.95% oxygen, 0.93% argon, 0.04% carbon dioxide, and small amounts of other gases [1]. The water vapour presence instead, is a variable component and it depends by the weather conditions and by the geographical position. The oxygen and the water vapour cause the greatest

percentage of the absorption due to gas between 10 and 100 GHz. The molecule of oxygen and the water molecule interact with the signal, this interaction cause a loss when the frequency of the radiowave is near to the resonance frequency of the molecule because, the molecule will try to align itself with the minimum potential with respect to the electric field. The resonance peaks of oxygen ($\sim$ 60 GHz) and water vapour ($\sim$ 22 GHz) between frequencies of 10 and 100 GHz are reported in figure 1.1

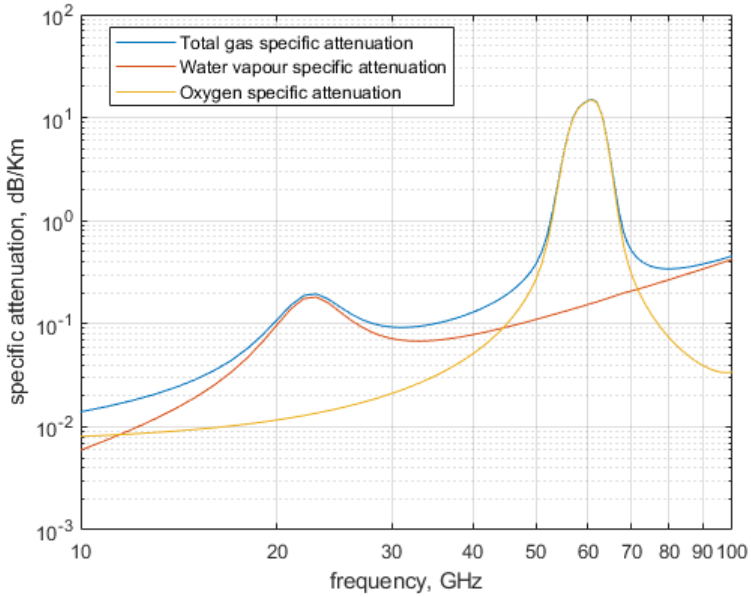

Figure 1.1: Specific gas attenuation due to oxygen and water vapour computed at $T = 15°C, P = 1013HPa, WV = 7.5g/m^3$

1.3. Water drop attenuation

Attenuation of electromagnetic waves by water drops such as rain and clouds, can cause serious degradation of communication systems [4]. The signal, when it hits the water drop, presents two principal effects: an energy loss due to Joule effect (the drop is absorbing part of the signal energy and then is dissipated as heat) and a scattering effect (the drop is scattering the signal in multiple directions).

1.3.1. Rayleigh and Mie scattering models

To study the effect of the hydrometeor on the signal it is necessary to study Joule and scattering effects together. First of all it is possible to model the hydrometeor as a "black box" sphere with a power input (the signal) and a power output (Joule and scattering effects):

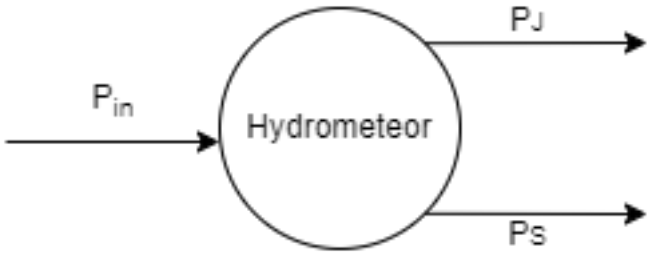

Figure 1.2: Hydrometeor black box model

The obtained equations are:

$$P_J = C_J S_i \tag{1.2a}$$

$$P_S = C_S S_i \tag{1.2b}$$

$$P_{IN} = C_{EXT} S_i \tag{1.2c}$$

$$C_{EXT} = C_J + C_{SC} \tag{1.2d}$$

Where C_{EXT} is the equivalent area of the droplet (total extinction section) and S_i is the incident power density.

Summing up, there is a dielectric sphere hit by a plan electromagnetic wave; thus it is possible to use the Mie's scattering model:

$$\begin{cases} \nabla^2 \mathbf{E} + n^2 k^2 \mathbf{E} = 0 \\ \nabla^2 \mathbf{H} + n^2 k^2 \mathbf{H} = 0 \end{cases} \tag{1.3}$$

$\mathbf{E}$ and $\mathbf{H}$ are the electric and magnetic field, k is the wave vector($k = \frac{2\pi}{\lambda}$) and n is the refractive index.
Defining a vector $\mathbf{M} = \nabla \times (r\xi)$ (with r position vector and ξ scalar variable), it is possible to demonstrate [8] that:

$$\nabla^2 \mathbf{M} + n^2 k^2 \mathbf{M} = \nabla \times (\nabla^2 \xi + n^2 k^2 \xi). \tag{1.4}$$

$\mathbf{M}$ satisfies the wave equation 1.3 when the right side of the equation 1.4 is equal to zero, so $\nabla^2 \xi + n^2 k^2 \xi = 0$. This last condition is verified when ξ is solution of the wave equation. Defining furthermore a vector $\mathbf{N} = \frac{1}{nk}(\nabla \times \mathbf{M})$, it is evident how $\mathbf{N}$ has the same property of $\mathbf{M}$.

Applying the correct boundary conditions the solution of 1.3 is given by:

$$\mathbf{E} = \mathbf{M}_v + i\mathbf{N}_u \tag{1.5a}$$

$$\mathbf{H} = m(-\mathbf{M}_u + i\mathbf{N}_v) \tag{1.5b}$$

where u and v are indipendent solutions of the scalar equation and m is the complex refractive index. It is possible to write the electric and the magnetic field as function of the ausiliary fields **M** and **N**. The sphere geometry hypotesis is now used again to write the plane wave in spherical coordinates:

$$u = e^{i\omega t}\cos\Phi\sum_{n=1}^{\infty} -a_n(-i)^n\frac{2n+1}{n(n+1)}P_n^l(\cos\theta)j_n(kr) \tag{1.6a}$$

$$v = e^{i\omega t}\sin\Phi\sum_{n=1}^{\infty} -b_n(-i)^n\frac{2n+1}{n(n+1)}P_n^l(\cos\theta)j_n(kr) \tag{1.6b}$$

where P_n^l are the Associated Legendre polynomials and j_n are the Bessel's spherical functions. Imposing the boundary conditions on the sphere's surface and introducing the parameter $x = \frac{2\pi a}{\lambda}$, the coefficients a_n and b_n are obtained:

$$a_n = \frac{\psi_n'(mx)\psi_n(x) - m\psi_n(mx)\psi_n'(x)}{\psi_n'(mx)\zeta_n(x) - m\psi_n(mx)\zeta_n'(x)} \tag{1.7a}$$

$$b_n = \frac{m\psi_n'(mx)\psi_n(x) - \psi_n(mx)\psi_n'(x)}{m\psi_n'(mx)\zeta_n(x) - \psi_n(mx)\zeta_n'(x)} \tag{1.7b}$$

where ψ and ζ are the Riccati-Bessel's function. The total cross section can be written in function of a_n and b_n:

$$C_{EXT} = \frac{2\pi}{k^2}\sum_{i=1}^{\infty}\left(|a_n|^2 + |b_n|^2\right) \tag{1.8}$$

When $|n|D \gg \frac{\lambda}{2\pi}$, with D diameter of the particle and λ the wavelength, the Mie's model can be simplified into the Rayleigh's model and it is possible to compute all the sections as:

$$C_S = \frac{8\pi}{3}\beta_0^4|\alpha_p|^2 \tag{1.9a}$$

$$C_{EXT} = \frac{4\pi}{\beta_0^2}Re\{S(0)\} \tag{1.9b}$$

$$C_J = \frac{\pi^2 Im(-K_w)}{\lambda} \sum_{n=1}^{N} D_n^3 \tag{1.9c}$$

where $S(0) = j\beta_0^3\alpha + \frac{2}{3}\beta_0^6\alpha_p^2$, K_w is proportional to the induced electric dipole moment of the drop, β_0 is the propagation constant and α_p represents the polarizability of the scatterer; α_p is function of n and D.
A visual representation of the Mie and the Rayleigh scattering is reported in the figure 1.3.

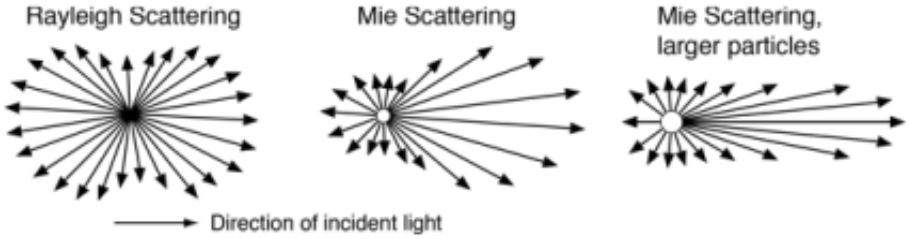

Figure 1.3: Rayleigh and Mie scattering

The Rayleigh condition is verified when the spheric geometry is respected, the scattering occurs in the far-region and the drop is way smaller than the wave length. Under this constraint the incident electric field will be a plane wave:

$$\vec{E}_S = \frac{e^{-j\beta_0 r}}{j\beta_0 r} S(\theta, \Phi, \psi)\vec{E}_{in} \tag{1.10}$$

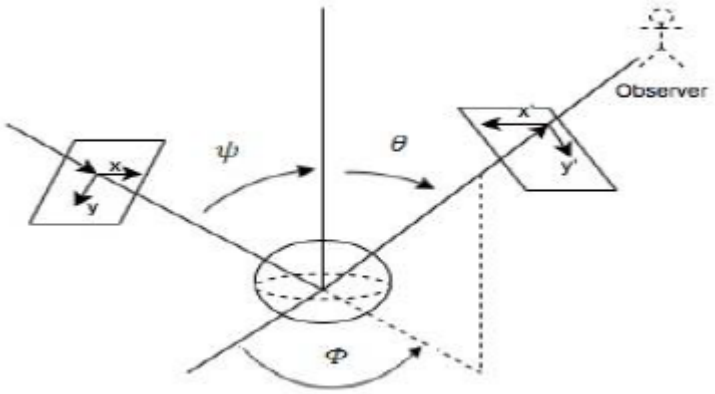

Figure 1.4: Geometry to study the attenuation due to water particles [5]

r is the distance from the observer and $S(\theta, \Phi, \psi)$ is the scattering matrix dependent on the dimension, the electric permittivity and the temperature of the particle.
For each particle the scatter section is:

$$\sigma_S = \lim_{r\to\infty} \frac{4\pi r^2 |E_s^2|}{|E_{in}^2|} \tag{1.11}$$

Substituting the 1.10 into 1.11

$$\sigma_S = \frac{4\pi}{\beta_0^2}|S| \tag{1.12}$$

is obtained.
The total scattered power (P_S) is computed integrating the pointing vector on the surface around the scatter:

$$P_S = C_S \frac{|E_{in}^2|}{\eta} \tag{1.13}$$

η represents the impedance the wave meets in the medium namely the integration of σ_S along the surface.
P_J, in the end, is computed as:

$$P_J = C_J \frac{|E_{in}^2|}{\eta} \tag{1.14a}$$

1.3.2. Cloud attenuation

Clouds are composed by small water drops (D$\sim \mu m$) for this reason it is possible to use the Rayleigh approximation.When drop diameters are small compared to the wavelength, the attenuation due to absorption becomes independent of drop size distribution and the attenuation depends on only the total columnar content of liquid water of the cloud L. It is possible to compute L from the radiometric measurements. Cloud attenuation is computed following the model presented in ITU-R P.840-8 [22]:

$$A_C = \alpha_L \frac{L}{\sin(\theta)} \tag{1.15}$$

where θ is elevation angle of the link and α_L is a coefficients depending on the frequency.

1.3.3. Rain attenuation

Rain attenuation represents the power loss due to a rain event. Raindrops can absorb, dissipate, depolarize, and scatter the propagated wave. This contribution is the prominent one for frequencies above 10 GHz. The power loss occurs in the same way as the cloud attenuation loss: absorption and scattering. The droplets composing the rain are way

bigger ($\sim$ mm) than the cloud's; for this reason it is not possible to use the Rayleigh approximation.
Mie model is very complex and it is not possible to apply it in a real situation of a rain event.
For this reason another model is used:
In order to compute the specific rain attenuation a volume of dimension x=1 m, y=1 m and thickness dz containing N water particles is created as reported in the figure 1.5:

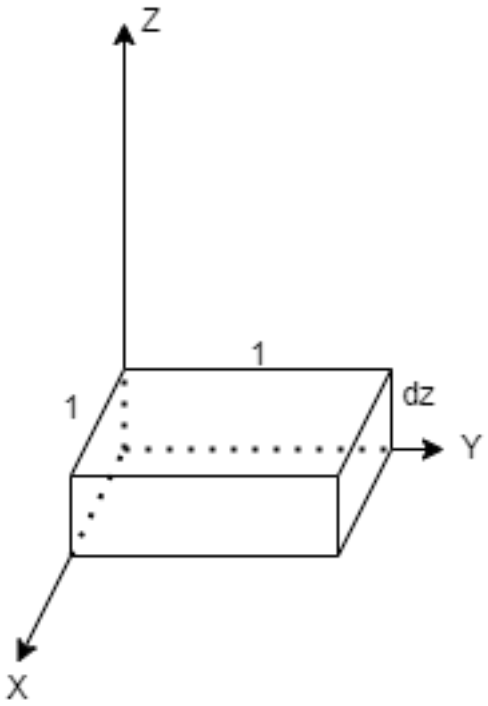

Figure 1.5: Volume dV which is containing N water particles

The electromagnetic wave goes through the 1 m^2 area and hit the hydrometeors, each drop has its own shape, dimension and orientation.
The power loss in the volume will be given by the following equation:

$$dP = -SC_{EXT}dV \;\Rightarrow\; dP = -SC_{EXT}dAdz,\; dA = 1 \;\Rightarrow\; dP = -SC_{EXT}dz \tag{1.16}$$

where S is the incident power density. The equation has a decreasing exponential solution:

$$S(z) = S(0)e^{-C_{EXT}Nz} \tag{1.17}$$

The rain slab is a dissipative medium and for this reason it is possible to write the general

formula of a power density of a wave in a this kind of material:

$$S(z) = S(0)e^{-2\alpha z} \tag{1.18}$$

Comparing the exponents of the equations 1.17 and 1.18 the specific rain attenuation is retrieved:

$$\gamma_R = \frac{1}{2} N C_{EXT} \quad [Np/m] \tag{1.19}$$

An important parameter to investigate the rain properties is the drop size distribution (DSD),N(D)dD, defined as the number of particles per cubic metre with a diameter comprised between D and D+dD.
The specific rain attenuation becomes:

$$\gamma_R = \frac{1}{2} \int_0^\infty N(D) C_{EXT}(D) dD \tag{1.20}$$

The DSD model is not always available, for this reason a relation between the specific rain attenuation and rain rate is investigated in past studies [18]:
It is possible to write the specific rain attenuation as

$$\gamma_R = kR^\alpha \tag{1.21}$$

where k and α coefficients can be computed in function of frequency, polarization angle and elevation angle from ITU-R P.838-3 [10].

2 | Mathematical and statistical tools

2.1. Complementary cumulative distribution function

In this thesis work to present results is widely used the complementary cumulative distribution function (ccdf) to present the results. To define it, it is easier passing through the definition of the cumulative distribution function (cdf). The ccdf will be, as the name says, its complementary function.
First of all a variable $\varkappa$ is defined. $\varkappa$ can be a scalar or a multi-dimensional array. Then a threshold $\bar{\varkappa}$ is created ($\varkappa$ and $\bar{\varkappa}$ must have the same dimension).
The cdf is a function F defined as follow:

$$F_{\varkappa} : \ \mathbb{R} \rightarrow [0, 1] \tag{2.1a}$$

$$F_{\varkappa} := P(\varkappa \leq \bar{\varkappa}) \tag{2.1b}$$

As last step it is applied the definition of complementarity at the cdf and the ccdf is obtained:

$$ccdf = 1 - cdf \ \Rightarrow \ \bar{F}_{\varkappa} = 1 - P(\varkappa \leq \bar{\varkappa}) \tag{2.2}$$

An example of a ccdf applied to a white noise is reported in figure 2.1.

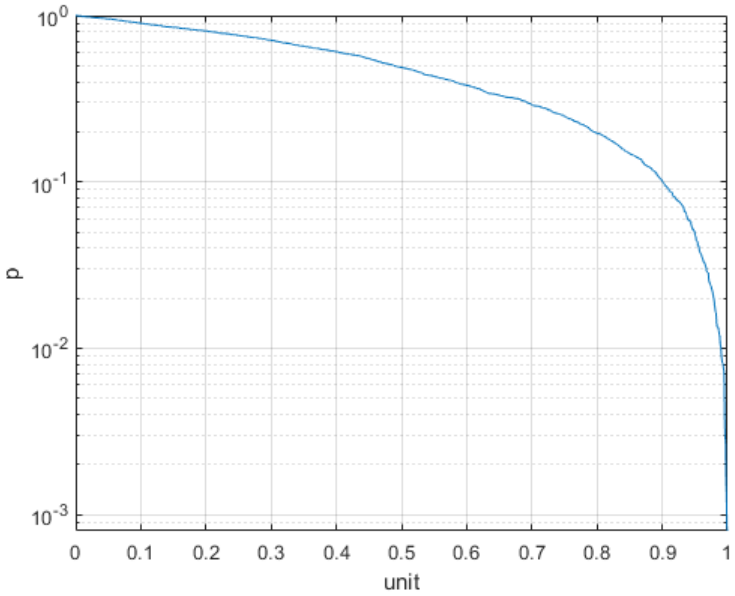

Figure 2.1: ccdf of a white noise

2.2. Mean value, standard deviation and root mean square value

To evaluate the goodness and the reliability of the results obtained from the scaling model implemented in this thesis the mean value (MV), the standard deviation (SD) and the root mean square value (RMS) are employed.
The MV is defined as:

$$\mu = \frac{1}{n}\sum_{i=1}^{n}(\varkappa_i) \tag{2.3}$$

It represents the average value of the distribution.
The SD is defined as:

$$\sigma = \sqrt{\frac{1}{n}\sum_{i=1}^{n}(\varkappa_i - \mu)} \tag{2.4}$$

It measures the dispersion of data with respect to the mean value.
The RMS is defined as:

$$\rho = \sqrt{\frac{1}{n}\sum_{i=1}^{n}(\varkappa_i^2)} \tag{2.5}$$

It is equal to write:

$$\rho = \sqrt{\mu^2 + \sigma^2} \tag{2.6}$$

3 | ITALSAT experiment

Italy's first operational communications satellite was launched 15 January 1991. Developed by a contractor team led by Alenia Spazio, ITALSAT carries ten active transponders plus five spares for 30/20 GHz and 50/40 GHz links. The 900 kg (on-station) spacecraft consists of a parallelepiped bus 2.3 m by 2.7 m by 3.5 m and two solar panels with a total span of 21.8 m and more than 1.5 kW power. The design life for the first test vehicle is of five years, it has been increased up to 8 years for the second ITALSAT. ITALSAT-2 was launched in 1996. It also carries ESA's first European Mobile Services (EMS) payload. ITALSAT-1 is stationed at 13.2 °E, it is also home of ITALSAT-2.
The satellites were moved to graveyard orbits in January 2001 and July 2002 respectively. [11]

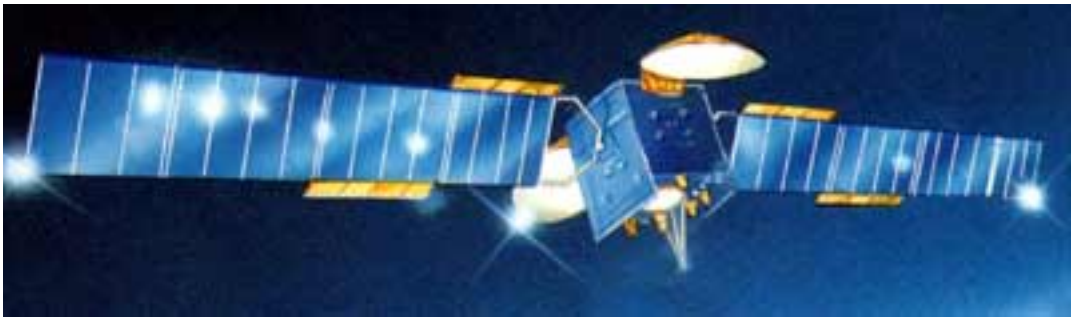

Figure 3.1: Rendering of ITALSAT-1 [11]

To have a better understanding of ITALSAT's orbit, a propagation with SGP4 starting from TLEs (which are reported in appendix A.1) is performed and the result is reported in figure 3.2

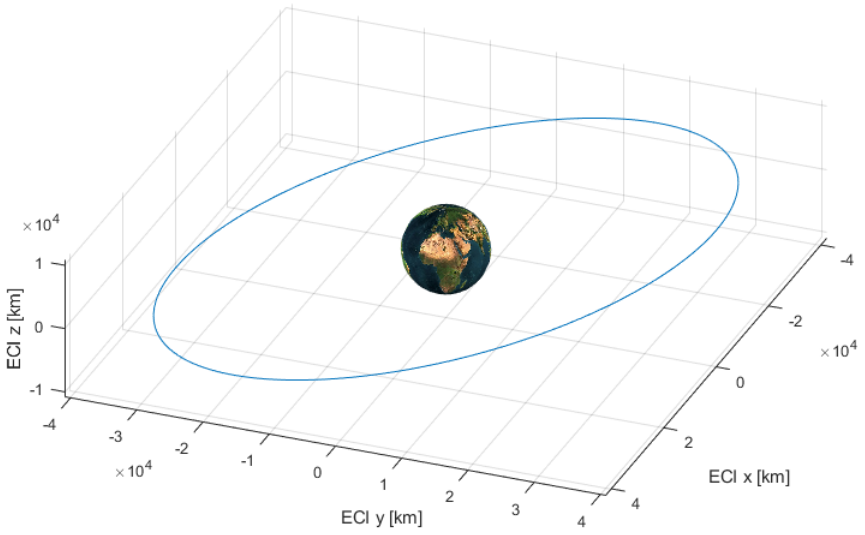

Figure 3.2: ITALSAT-1 orbit

Orbital parameters for ITALSAT-1 are listed in table 3.1

Table 3.1: ITALSAT-1 orbital parameter

NORAD ID:	24208
Perigee:	35541.1 km
Apogee:	35753.5 km
Inclination:	13.2°
Period:	1428.7 minutes
Semi major axis:	42020 km

ITALSAT characteristics and equipment are resumed in the table 3.2

Table 3.2: ITALSAT data

Nation:	Italy
Type / Application:	Communication
Operator:	-
Contractors:	Alenia Spazio
Equipment:	9 (+6) Ka-band transponders (both), Ka-band propagation beacon (#1), L-band, Ku-band transponder
Configuration:	GeoBus (ITALSAT Bus)
Propulsion:	R-4D-11
Power:	2 deployable solar arrays, batteries
Lifetime:	6 years (#1), 8 years (#2)
Mass:	1850 kg (#1), 1983 kg (#2)
Orbit:	GEO

ITALSAT is communicating with Spino d'Adda Earth station which installed instruments can be retrieved in the table 3.3

Table 3.3: Spino d'Adda instruments data [12]

Beacons' freq. [GHz]	18.7 - 39.6 - 49.5
polarization	V - C - V\H
Latitude	45.4°N
Longitude	9.5°E
Altitude a.m.s.l. [m]	84
Elevation of the link	37.8°
Antenna diam. [m]	3.5
Sampl. rate [Hz]	1

3.1. Dataset

The data used in this thesis are from the biennium 1995-1996 and they are characterized by:
One data point per second for:

- Total attenuation.

One data point per minute for:

- Meteorological data:
  - Temperature in °C (T)
  - Total pressure in hPa (P)
  - Relative humidity in % (RH)
  - Wind intensity and direction are provided too but they are not used in this thesis.
- Rain measurements.

To homogenise the data and reduce the computation time, total attenuation measurements are converted into the same format of the meteorological data.
To perform that operation, the 86400 points (for each day) are subdivided into 1440 groups with 60 elements; each group and the mean value of the group is taken.
An example of this operation is reported in the figure 3.3

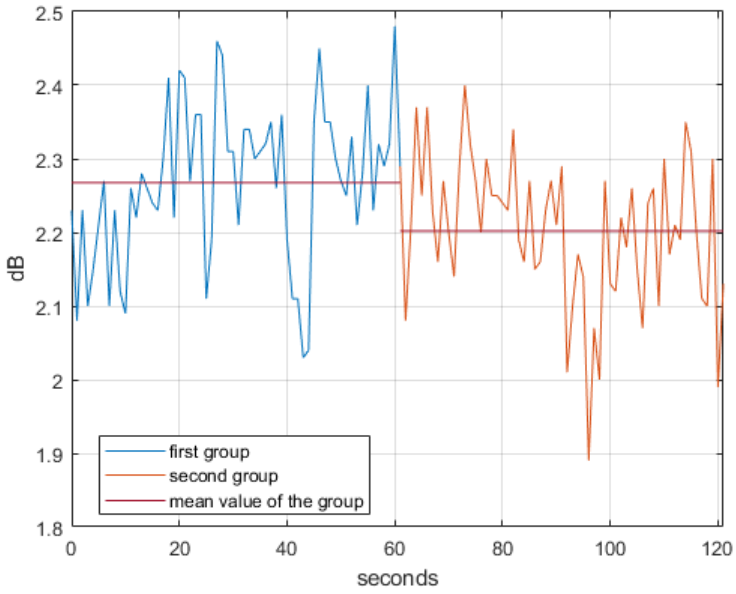

Figure 3.3: Mean value of the group

4 | Attenuation computation

The aim of this thesis is to perform a frequency scaling from Ka to EHF bands of the rain attenuation part. To do that the first, necessary, step is to have a reliable dataset representing the real rain attenuation. It is not a trivial task isolating only the contribution from rain and the way adopted in this thesis to retrieve this kind of data, it is to compute each component of the total attenuation vector at 18.7, 39.6 and 49.5 GHz.

4.1. Scintillations computation

The scintillations part is present on the dataset of the total attenuation retrieved form ITALSAT. This contribution it is not directly computed but filtered out with a moving average filter. The cut-off frequency of the filter used is equal to 0.03 Hz. The comparison between total attenuation data at 39.6 GHz with and without scintillations is reported in the figure 4.1, for the whole day of 2 january 1995. The filtering operation is the first one in order to "clean up" the datasets

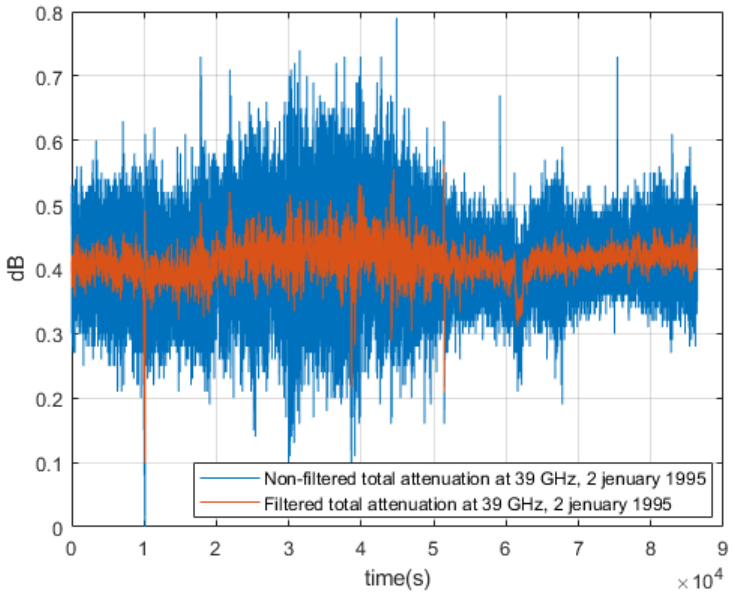

Figure 4.1: Total attenuation at 39.6 GHz with and without filtering out the scintillations

4.2. Gas attenuation computation

The gas contribution is computed using the ITU-R P.676-13 model [2], the specific gas attenuation is retrieved with the equation 4.1. It is summed up the specific attenuation of oxygen and the specific attenuation of water vapour.

$$\gamma = \gamma_{ox} + \gamma_{wv} = 0.1820 f \left(N''_{ox} + N''_{wv}\right) \tag{4.1}$$

where:

- f is the frequency
- $N''_{ox}(f)$ and $N''_{wv}(f)$ are the imaginary parts of the frequency-dependent complex refractivities, such that

$$N''_{ox}(f) = \sum_{i(ox)} S_i F_i + N''_D(f) \tag{4.2}$$

and

$$N''_{wv}(f) = \sum_{i(wv)} S_i F_i \tag{4.3}$$

The line strength S_i is computed as:

$$S_i = a_1 10^7 p \theta^3 exp^{a_2(1-\theta)} \quad for\ oxygen \tag{4.4}$$

$$S_i = b_1 10^{-1} e \theta^{3.5} exp^{b_2(1-\theta)} \quad for\ water\ vapour \tag{4.5}$$

where:

  - e, water vapour partial pressure (hPa)
  - p, is the dry air pressure (hPa)
  - θ, 300/T, T is the temperature in K

e,p and T are derived from meteorological dataset:
T is directly available from the data (in °C, so it is necessary to add 273.15 to obtain the temperature in K). The water vapour partial pressure, e, at any altitude may be obtained from the water vapour density (ρ), and the temperature, T (K), at that altitude using the expression reported in 4.6

$$e = \rho \frac{T}{216.7} \tag{4.6}$$

the meteorological data gives the total air pressure and the relative humidity, to obtain the water vapour density is used the equation 4.7

$$\rho = RH\frac{VD}{100} \tag{4.7}$$

where VD is function of t (temperature in °C) and it is computed as:

$$VD(t) = 5.018 + 0.3231t + 8.1847 \cdot 10^{-3}t^2 + 3.1243 \cdot 10^{-4}\ t^3 \tag{4.8}$$

In the end the dry air pressure is computed subtracting from the total air pressure the water vapour pressure as reported in equation 4.9.

$$p = P - \rho \tag{4.9}$$

To compute F_i the next equation is followed:

$$F_i = \frac{f}{f_i}\left[\frac{\Delta f - \delta(f_i - f)}{(f_i - f)^2 + \Delta f^2} + \frac{\Delta f - \delta(f_i + f)}{(f_i + f)^2 + \Delta f^2}\right] \tag{4.10}$$

where

$$\begin{cases} \Delta f = a_3 10^4 (p\theta^{(0.8-a_4)} + 1.1e\theta) \quad for\ oxygen \\ \Delta f = b_3 10^4 (p\theta^{b_4} + b_5 e\theta^{b_6} \quad for\ water\ vapour \end{cases} \tag{4.11}$$

δ is a correction factor and it is computed as:

$$\begin{cases} \delta = (a_5 + a_6\theta)10^4(p+e)\theta^{0.8} \quad for\ oxygen \\ \delta = 0 \quad for\ water\ vapour \end{cases} \tag{4.12}$$

The coefficients a_i ,b_i and f_i are tabulated in the tables A.1 for oxygen and A.2 for water vapour in the appendix A.

The results obtained for the gas attenuation part at 18.7, 39.6 and 49.5 GHz are reported in figure 4.2 in ccdf form.

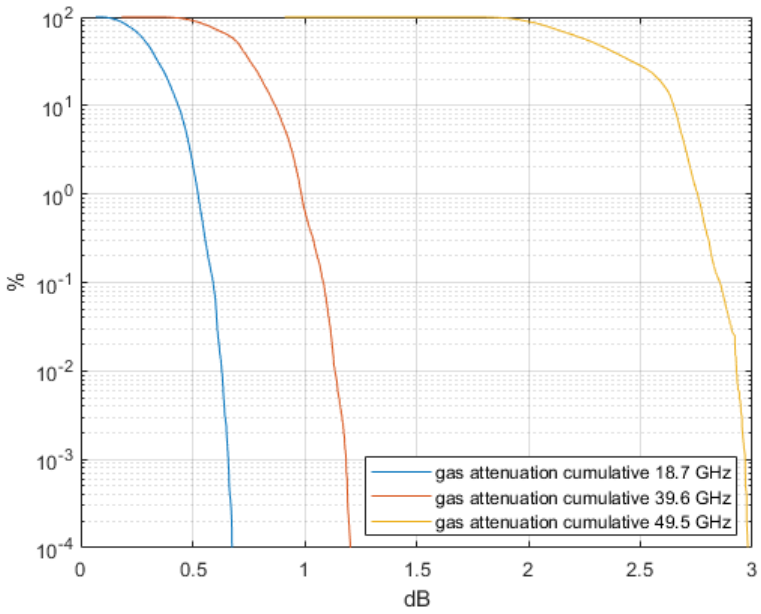

Figure 4.2: Gas attenuation in ccdf form at 18.7, 39.6 and 49.5 GHz

4.3. Cloud and Rain attenuation computation

To isolate the rain part from the cloud part it is not a easy procedure, in this thesis is implemented the methodology presented in "Enhancement of the Synthetic Storm Technique for the Prediction of Rain Attenuation Time Series at EHF" [3].
First of all the excess attenuation A_{RC} (representing the cloud and rain attenuation both) is computed subtracting from the total attenuation the gas contribution:

$$A_{RC} = A_{TOT} - A_{GAS} \tag{4.13}$$

Then the instantaneous discrimination ratio R_{RC} is evaluated as:

$$R_{RC} = aexp(-bA_{RC}) + (1-a)exp(-cA_{RC}) \tag{4.14}$$

The correlation between the excess attenuation and the instantaneous discrimination factor is a monotonically decreasing exponential (as reported in the figure 4.3): when the link is about to enter in the rain cell the attenuation will be caused only by the clouds ($R_{RC} = 1,\ A_R = 0$), as the rain event increases its presence on the link R_{RC} decreases its value and the rain attenuation takes over as dominant attenuation in the A_{RC}.

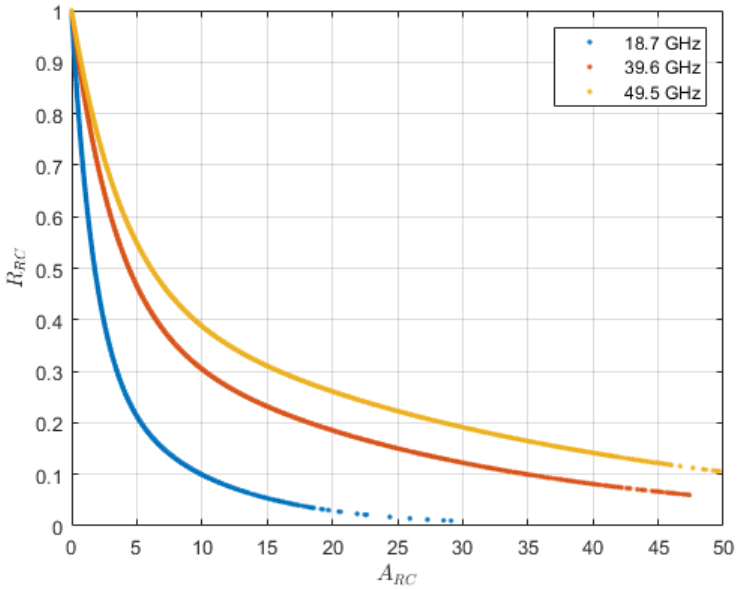

Figure 4.3: Trend of R_{RC} in function of A_{RC}

The last step to get the cloud attenuation and the rain attenuation is presented in the equations 4.15 and 4.16:

$$A_C = \begin{cases} R_{RC} A_{RC} & if\ A_{RC} \leq A_{RC}^{max} \\ A_C^{max} & if\ A_{RC} > A_{RC}^{max} \end{cases} \tag{4.15}$$

$$A_R = A_{RC} - A_C \tag{4.16}$$

The coefficients a,b,c and A_{RC}^{max}, A_C^{max} depend from the frequency and their value is reported in the table 4.1.

Table 4.1: cloud coefficients

	a	b	c	A_C^{max} [dB]	A_{RC}^{max} [dB]
18.7 GHz	0.676	0.5905	0.12	1.1	11
39.6 GHz	0.5830	0.3065	0.04087	3.85	16.9
49.5 GHz	0.53	0.26	0.03	5.8	30

"Enhancement of the Synthetic Storm Technique for the Prediction of Rain Attenuation Time Series at EHF" proposes the coefficients for the frequency of 19.7 and 39.4 GHz. To compute the coefficients for the frequencies of interest (18.7, 39.6 and 49.5 GHz),

it is made a minimization of the difference between the ccdf of the cloud attenuation (from the equation 4.15) and the one estimated from radiosonde observations (RAOBS), collected at Milano-Linate airport using P-RH-T vertical profiles to derive the liquid water content by means of the TKK cloud detection algorithm. The cloud attenuation of comparison is calculated through the Liebe MPM93 model. The comparison between the cloud attenuation from equation 4.15 and the one from RAOBS data is reported in figure 4.4 for the three frequencies, in ccdf form. Also the therm A_C^{MAX} is retrieved from the cloud attenuation derived with RAOBS data: A_C^{MAX} is set as the value reached from the ccdf exceeding the probability of 0.01%.

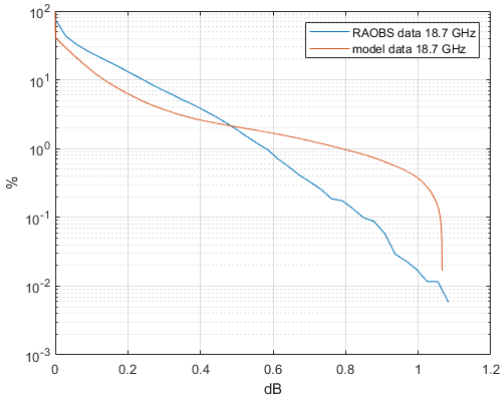

(a) Cloud attenuation in ccdf form, model and RAOBS data at 18.7 GHz.

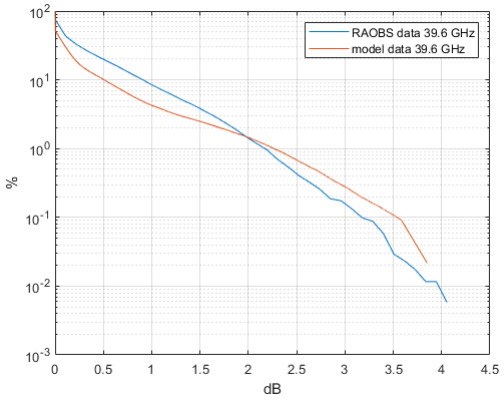

(b) Cloud attenuation in ccdf form, model and RAOBS data at 39.6 GHz.

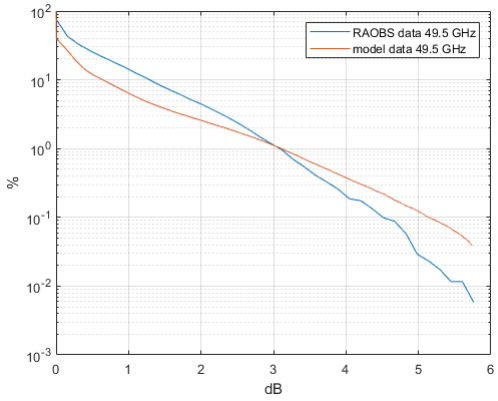

(c) Cloud attenuation in ccdf form, model and RAOBS data at 49.5 GHz.

Figure 4.4: comparison between RAOBS cloud attenuation and cloud attenuation from the thesis model

The cloud attenuation and rain attenuation obtained for the frequencies of 18.7, 39.6

and 49.5 GHz are reported in the figure 4.5 and in figure 4.6 in ccdf form. In the figure 4.5 above the attenuation of 35 dB, the rain attenuation ccdf for the frequency of 39.6 GHz is over the 49.5 one because the lacking of data: the low number of data causes the "steps" of the ccdf. Another cause is associated to the limitations in the derivation of rain attenuation using the proposed model, as well as to the fact that, close to the receiver dynamic range, mesurements are more affected by noise. These two effects lead to the misleading graphical behavior.

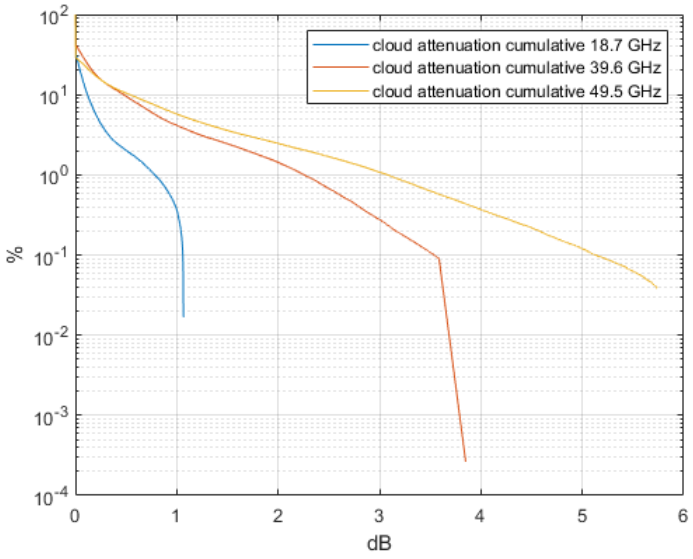

Figure 4.5: Cloud attenuation in ccdf form at 18.7, 39.6 and 49.5 GHz

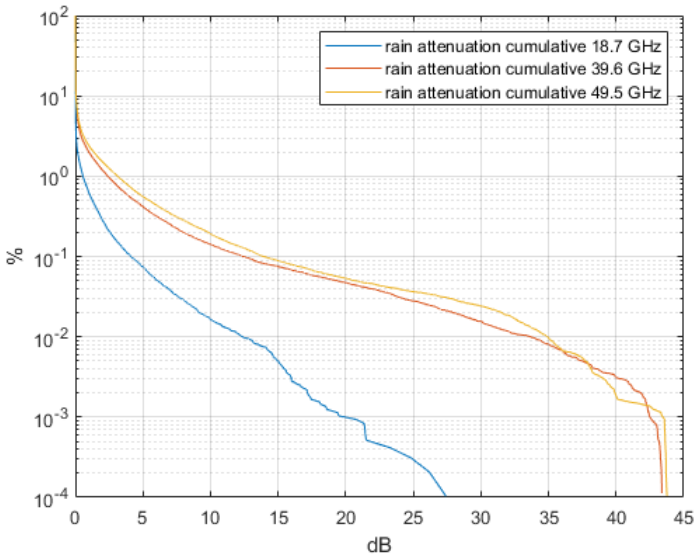

Figure 4.6: Rain attenuation in ccdf form for 18.7, 39.4 and 49.5 GHz

4.4. Overall attenuation

All the effects that are reducing the power of the signal due to tropospheric effects have been computed, a resuming work flow of the process followed is presented in the figure 4.7

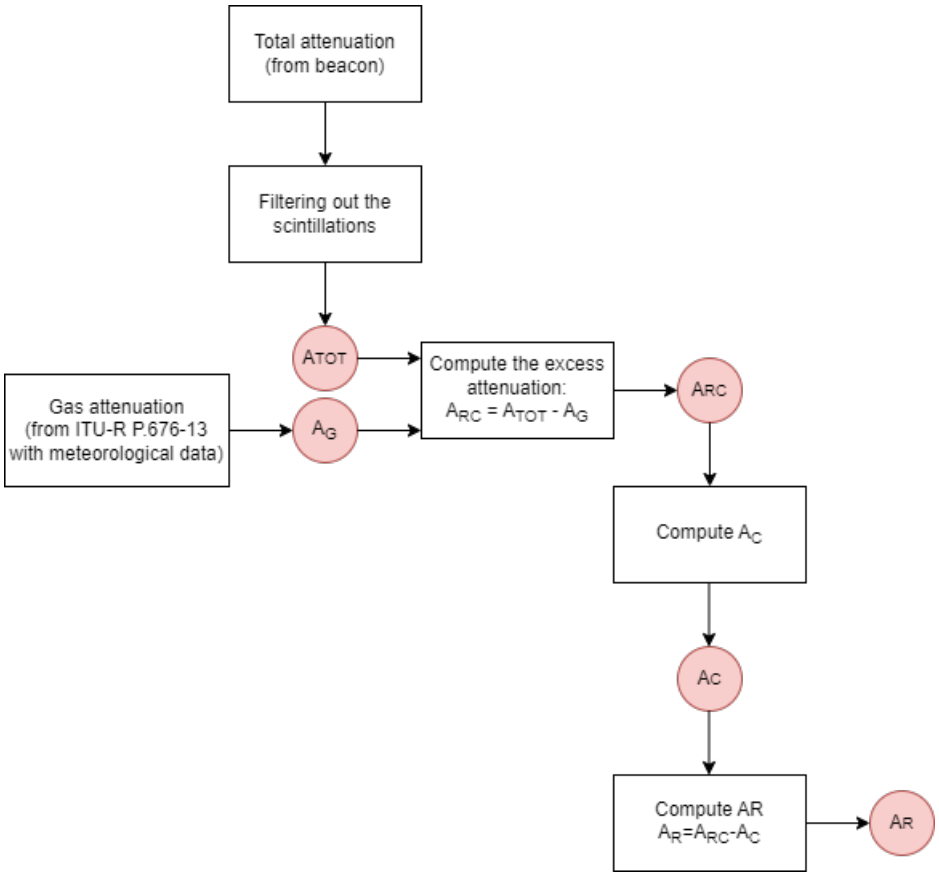

Figure 4.7: Workflow for the separation of total attenuation into its contributions

The figures 4.8 and 4.9 report every attenuation component retrieved from the methods in ccdf form and for a day (1 data-point per minute) at the frequencies of 18.7, 39.6 and 49.5 GHz.

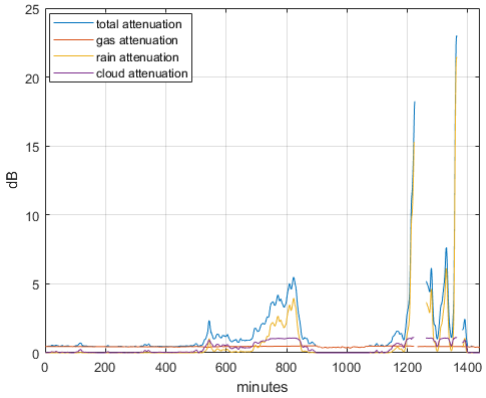

(a) Total attenuation and its component at 18.7 GHz, 26 may 1995.

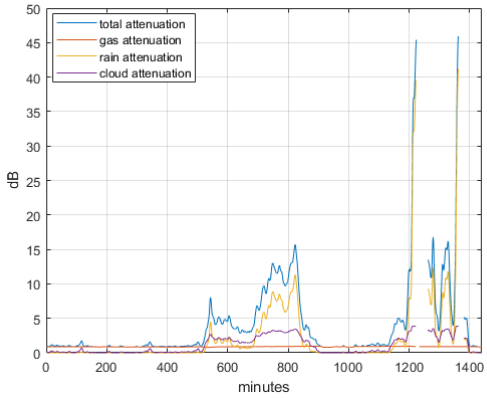

(b) Total attenuation and its component at 39.6 GHz, 26 may 1995.

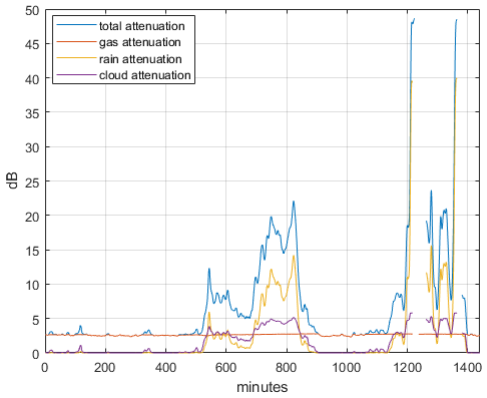

(c) Total attenuation and its component at 49.5 GHz, 26 may 1995.

Figure 4.8: Every attenuation component for the frequencies of 18.7, 39.6 and 49.5 GHz for the 26 may 1995

The figure 4.8 presents some "holes", these holes represent a missing data. This is due because the attenuation value goes beyond the dynamic range of the receiver and the data is interpreted as a `NaN` by `Matlab`. This issue is not present in the results in ccdf form because the `NaN` values are ignored by the function.

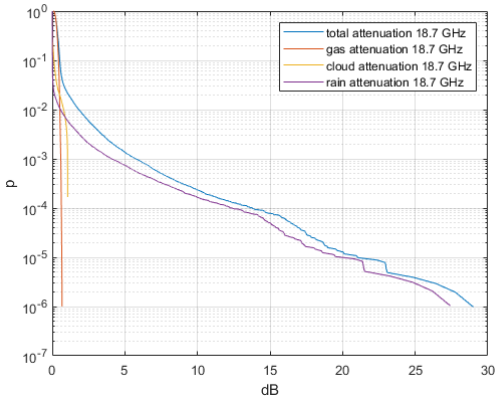

(a) Total attenuation and its component at 18.7 GHz.

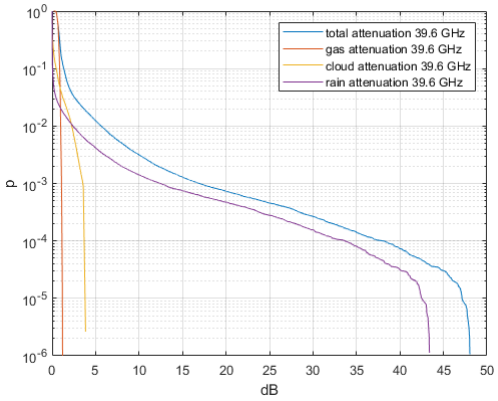

(b) Total attenuation and its component at 39.6 GHz.

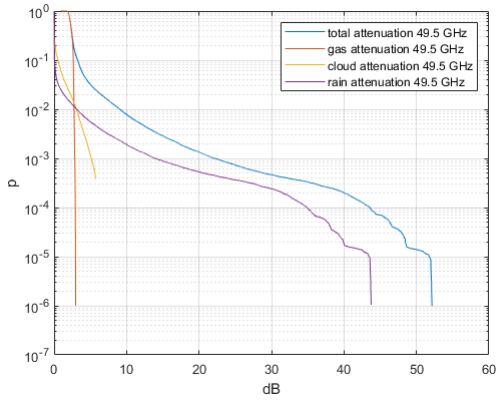

(c) Total attenuation and its component at 49.5 GHz.

Figure 4.9: Every attenuation component for the frequencies of 18.7, 39.6 and 49.5 GHz in ccdf form

5 | Frequency scaling

The frequency scaling technique (FS) is a methodology used to predict an attenuation at the frequency f_2 (higher frequency) starting from a frequency f_1 (lower frequency). It is possible to perform the FS for all kind of attenuations.To achieve the frequency scaling of the rain attenuation (which causes major attenuation of the propagated radio waves in terrestrial and satellite communication links) it is possible to proceed with two different approaches; the first one is based on empirical relationship of a satellite link for two channels through approximating the ratio $\left(\frac{f_2}{f_1}\right)^n$, n is a numerical coefficient that belong to an interval between 1.72 and 2.0 [19]. The second approach instead is based on physical formulation of the attenuation of interest. This is a more physically sound approach, i.e. on an expression aimed at modeling rain attenuation starting from the rain rate.
The motivations behind applying the frequency scaling are several:

- EHF bands permit to exchange a high amount of data in the link but these frequencies have the wavelength in the same order of magnitude of raindrops (mm) for this reason the signal is highly disturbed by the precipitation events. For this reason during the design phase of the system a reliable rain altitude prediction model is necessary. The rain attenuation behaviour is well known at some frequencies and a reliable model to estimate this attenuation already exists. The frequency scaling permits to use the information coming from these models (or from link measurements) and use them as a trustworth reference.

- Frequency scaling techniques can be helpful to estimate the attenuation at another frequency band for the quick management of terrestrial and slant links. In addition, real-time frequency attenuation scaling can be used in adaptive fade mitigation systems [20].

The purpose of this thesis, it is to implement a valid, accurate and easy model, based on the physical process of the problem. This method is based on the minimization of the error, between the real rain attenuation A_R (retrieved from the first thesis part) and the estimated rain attenuation ($\tilde{A}_R$) which can be computed as:

$$\tilde{A}_R(f,\tau,\theta) = k(f,\tau,\theta)R^{\alpha(f,\tau,\theta)}PRF \tag{5.1}$$

The coefficientsα and k are obtained following the methodology illustrated in ITU-R P.838-3 [10]; they are function of the frequency, the elevation angle and the polarization angle. R is the rain rate [mm/h] and PRF is the path reduction factor: PRF represents the ratio of the effective path length of a link where the rain rate is considered as uniform [21], to that of the actual link length. It accounts for the inhomogeneity of the spatial form of rain along a given path.
The error can be written as:

$$\epsilon = |A_R - \tilde{A}_R| \;\Rightarrow\; \epsilon = |A_R - kR^{\alpha}PRF| \tag{5.2}$$

Finding the optimal R and the optimal PRF it is not a trivial task: there is a single equation in two different unknowns. The approach employed is a "brute force" method: a double for cycle is used to find the best couple of R and PRF such that the error ϵ is minimized. The script used is reported in the appendix B.
All the elements are now available to perform the frequency scaling:
First of all best the scaling factor is computed with the equation 5.3

$$R_{SF} = \frac{k(f_2)R^{\alpha}(f_2)PRF}{k(f_1)R^{\alpha}(f_1)PRF} \tag{5.3}$$

Then the rain attenuation at the frequency f_2 is computed starting from the rain attenuation at frequency f_1 multiplying it with the scaling factor, as reported in equation 5.4

$$A_R(f_2) = R_{SF}A_R(f_1) \tag{5.4}$$

In the equation 5.3 PRF does not give a real contribution because it is elided during the ratio operation. However it is important compute it to check if the frequency scaling method is maintaining the physics of the rain attenuation. PRF's value is usually, some kilometres. In this work is used a PRF values that belongs to an interval within between 0 and 10 km.
The R and PRF gotten from the minimization method are do not have a physical value: they are the best coefficients that minimize ϵ but the method is not able to choose the physical R and PRF couple; anyway the method respect the logic to have a monotonically decreasing trend of the couple R-PRF: when R is high PRF is low and vice versa. This relation is reported in the figure 5.1 as obtained by applying the minimization to the data.

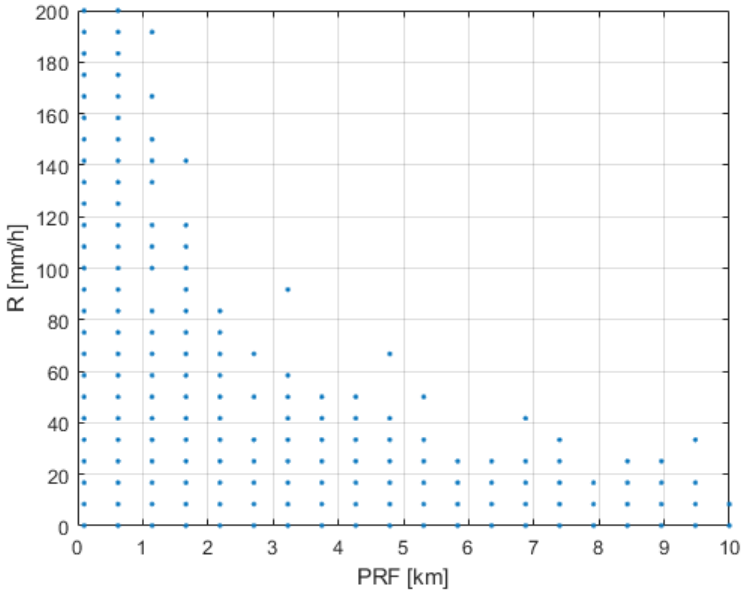

Figure 5.1: Relation between R and PRF obtained from the minimization of ϵ

The results obtained with the phisically based frequency scaling (PBFS) are compared with the well known and consolidated Drufuca's method.

5.1. Scaling operation

Drufuca scaling model has been implemented by G.Drufuca in 1974 [6]. It belongs to the family of empirical scaling methods. It works pretty well when the frequency of the signal is between 11 and 19 GHz [13]. As mentioned before this scaling is based on the ratio between the frequency f_2 and f_1 exponentiated by a coefficients $n = 1.72$, the formula is reported in the equation 5.5

$$A_R(f_2) = \left(\frac{f_2}{f_1}\right)^{1.72} A_R(f_1) \tag{5.5}$$

The scaling with this method is carried out in three different ways:

1) From 18.7 to 39.6 GHz
2) From 18.7 to 49.5 GHz
3) From 39.6 to 49.5 GHz

The results of this scaling are presented in the figure 5.2 for the first case, in figure 5.3 for the second and in 5.4 for the last one. They are reported in ccdf form and for a a sample

day (1 data-point per minute).

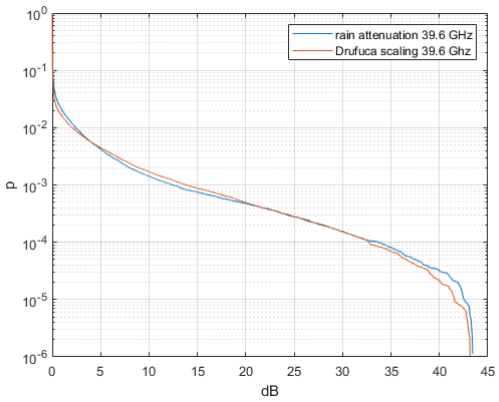

(a) Frequency scaling from 18.7 to 39.6 GHz in ccdf form.

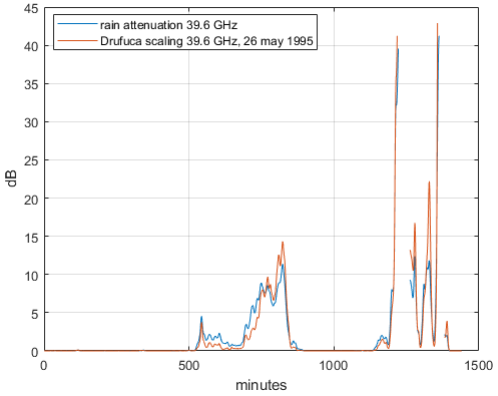

(b) Frequency scaling from 18.7 to 39.6 GHz, 26 may 1995.

Figure 5.2: Drufuca scaling from 18.7 to 39.6 GHz

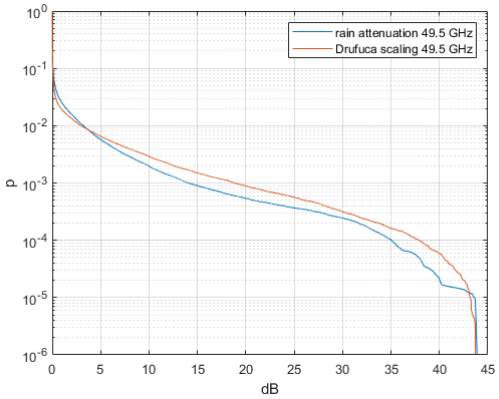

(a) Frequency scaling from 18.7 to 49.5 GHz in ccdf form.

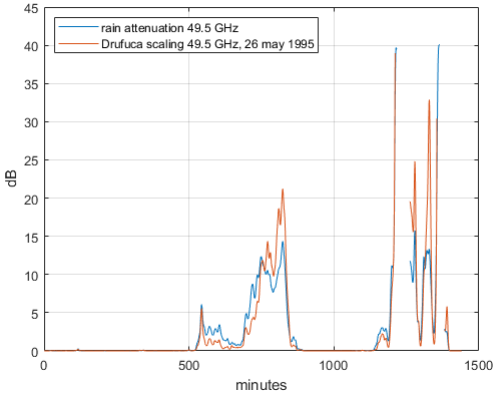

(b) Frequency scaling from 18.7 to 49.5 GHz, 26 may 1995.

Figure 5.3: Drufuca scaling from 18.7 to 49.5 GHz

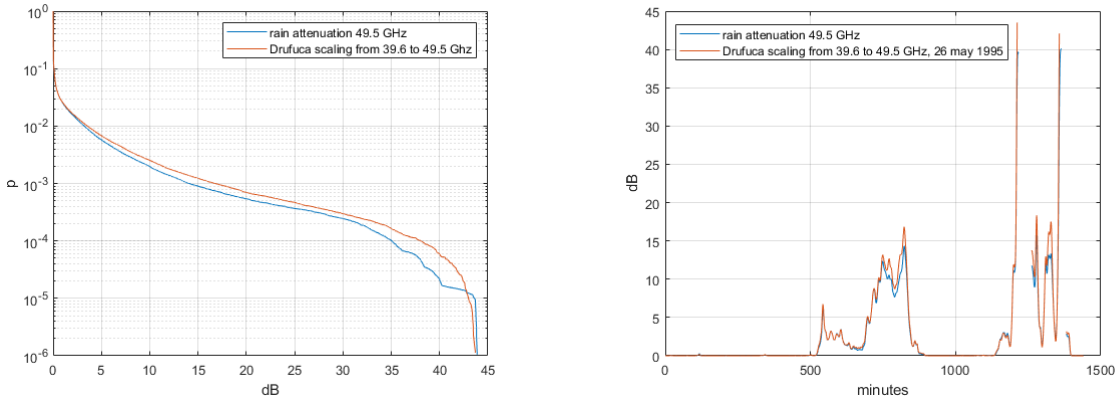

(a) Frequency scaling from 39.6 to 49.5 GHz in ccdf form.

(b) Frequency scaling from 39.6 to 49.5 GHz, 26 may 1995.

Figure 5.4: Drufuca scaling from 39.6 to 49.5 GHz

As it is possible to observe from the figures Drufuca's scaling method works good when the frequencies of interest are near each other. When the frequency increases and the attenuation value is high the method loses quality.

The scaling is now performed with the PBFS method; also in this case it is carried out from 18.7 GHz to 39.6 and 49.5 GHz and from 39.6 GHz to 49.5 GHz. The results are presented in the figures 5.5 (18.7 to 39.6 GHz) 5.6 (18.7 to 49.5 GHz) and 5.7 (39.6 to 49.5 GHz) in ccdf format and for one day (one point per minute).

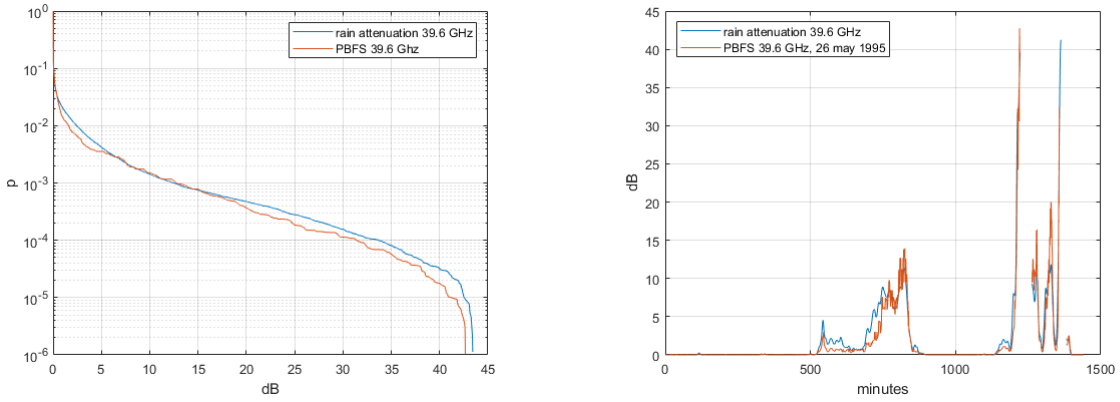

(a) Frequency scaling from 18.7 to 39.6 GHz in ccdf form.

(b) Frequency scaling from 18.7 to 39.6 GHz, 26 may 1995.

Figure 5.5: PBFS from 18.7 to 39.6 GHz in ccdf form and for 26 may 1995

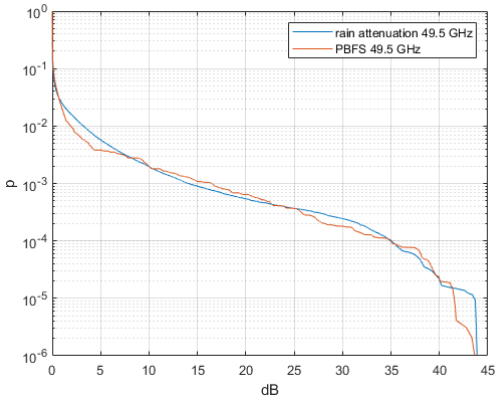

(a) Frequency scaling from 18.7 to 49.5 GHz in ccdf form.

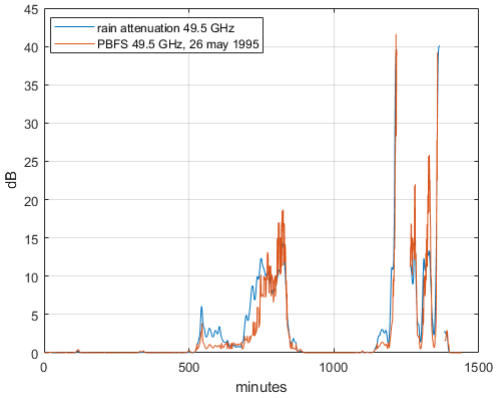

(b) Frequency scaling from 18.7 to 49.5 GHz, 26 may 1995.

Figure 5.6: PBFS from 18.7 to 49.5 GHz in ccdf form and for 26 may 1995

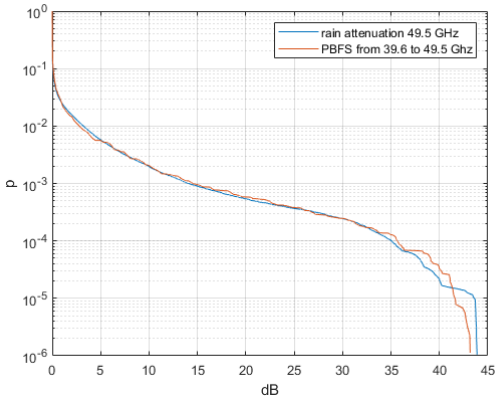

(a) Frequency scaling from 39.6 to 49.5 GHz in ccdf form.

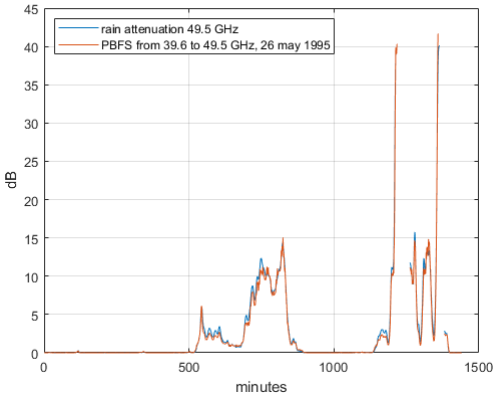

(b) Frequency scaling from 39.6 to 49.5 GHz, 26 may 1995.

Figure 5.7: PBFS from 39.6 to 49.5 GHz in ccdf form and for 26 may 1995

The results obtained from the PBFS method are very good when the scaling goes from 39.6 to 49.5. In the scaling from 18.7 to 39.6 GHz and from 18.7 to 49.5 GHz an "oscillation" of the scaled ccdf is present, it is possible to reduce this behaviour increasing the grid density of R and PRF.

5.2. α and k optimization

In the PBFS method α and k coefficients are computed with methodology presented in ITU-R P.838 [10] and they are not based on the DSD of the rain event that is actually disturbing the link. To improve the accuracy of the method it is possible to use a DSD model [15] which gives twelve possible $\alpha - k$ couple for the instant rain attenuation. The minimization problem will be the same but now there are three variable (R, PRF and the couple $\alpha - k$ and one equation (eq. 5.2). The approach implemented is again a brute-force one with a triple for cycle. Due to the extra dimension added, the script is more hardware demanding. To maintain the same grid density for R and PRF with respect to the PBFS method without the α and k optimization and keep the two methods comparable each other, a workstation (courtesy of DEIB labouratory) is used. The results are reported in ccdf and for one day (one point per minute) in figures 5.8, 5.9 and 5.10. Also in this case the scaling is performed from 18.7 to 39.6 GHz, from 18.7 to 49.5 GHz and from 39.6 to 49.5 GHz.

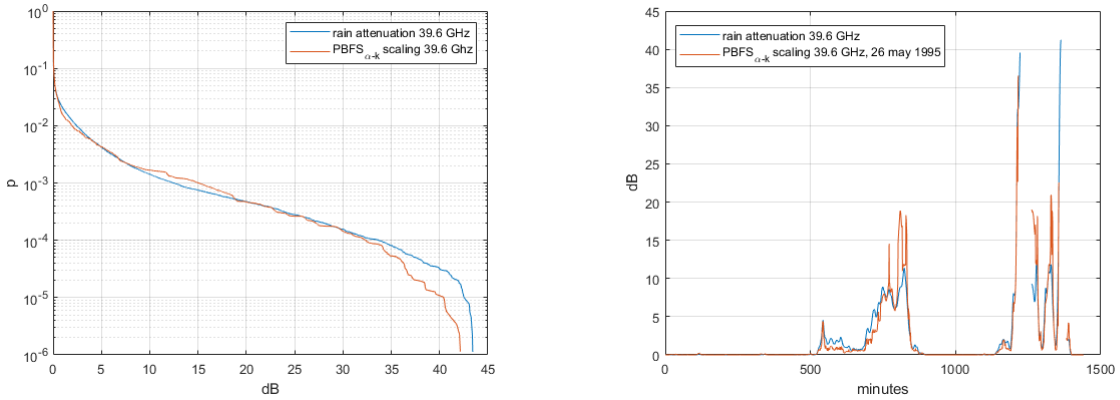

(a) Frequency scaling from 18.7 to 39.6 GHz in ccdf form.

(b) Frequency scaling from 18.7 to 39.6 GHz, 26 may 1995.

Figure 5.8: PBFS with α an k optimization from 18.7 to 39.6 GHz in ccdf form and for 26 may 1995

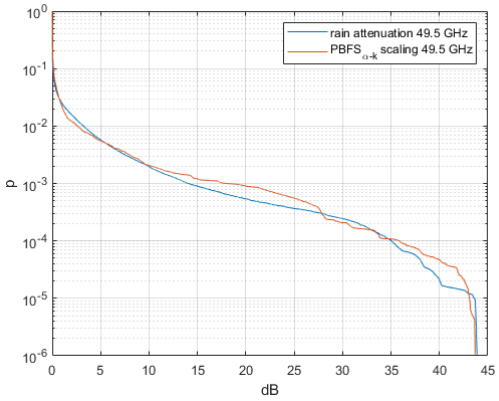

(a) Frequency scaling from 18.7 to 49.5 GHz in ccdf form.

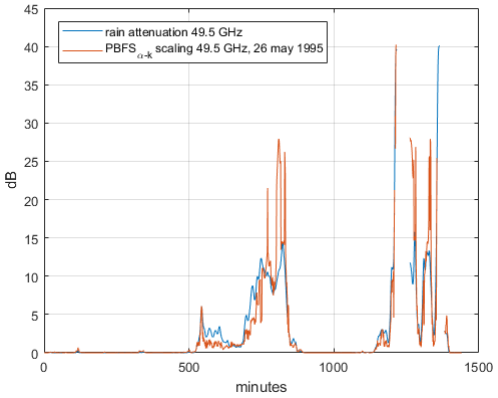

(b) Frequency scaling from 18.7 to 49.5 GHz, 26 may 1995.

Figure 5.9: PBFS with α an k optimization from 18.7 to 49.5 GHz in ccdf form and for 26 may 1995

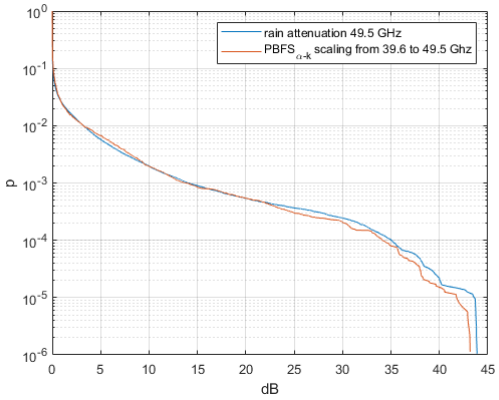

(a) Frequency scaling from 39.6 to 49.5 GHz in ccdf form.

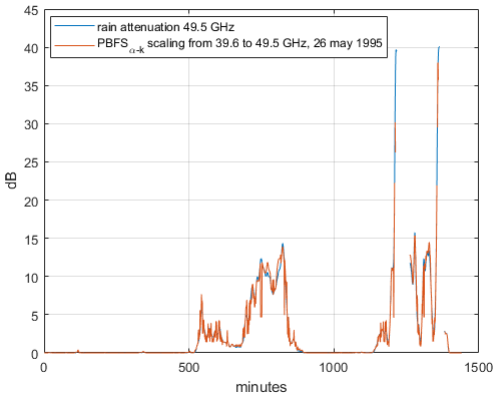

(b) Frequency scaling from 39.6 to 49.5 GHz, 26 may 1995.

Figure 5.10: PBFS with α an k optimization from 39.6 to 49.5 GHz in ccdf form and for 26 may 1995

5.3. Results

The statistical analysis of the results obtained is performed on the ccdf of the rain attenuation over the biennium of interest of the dataset. To perform the analysis recommendation ITU-R P.311-18 [14] error figure is adopted. The procedure presented in the ITU-R P.311-18 is composed by 5 steps:

1) Sample the attenuation CCDF at fixed values. In this thesis, probability levels equally spaced in the logarithmic scale from 0.001% to 100% are selected. The floor value is selected to avoid the statistical instability of the ccdf.

2) The ratio between scaled data and real data is computed for each percentage of time:

$$R_i = \frac{A_{SCALED,i}}{A_{REAL,i}} \tag{5.6}$$

3) The variable $\varkappa$ is calculated as:

$$\begin{cases} \varkappa = \log(R_i) \left(\frac{A_{REAL,i}}{10}\right)^{0.2} & if\ A_{REAL,i} < 10dB \\ \varkappa = \log(R_i) & if\ A_{REAL,i} \geq 10dB \end{cases} \tag{5.7}$$

This operation is repeated for each probability level.

4) The MV, SD and RMS of the variable $\varkappa$ are computed as reported in the section 2.2

The results of the mean value and the root mean square of the drufuca scaling method, PBFS method and the PBFS method with α and k optimization are reported in the tables 5.1, 5.2 and 5.3

Table 5.1: RMS and MV of Drufuca method

	RMS	MV
18.7 to 39.6 GHz	0.1646	-0.0740
18.7 to 49.5 GHz	0.1936	0.0231
39.6 to 49.5 GHz	0.1010	0.0871

Table 5.2: RMS and MV of PBFS method

	RMS	MV
18.7 to 39.6 GHz	0.1552	-0.0839
18.7 to 49.5 GHz	0.1874	-0.0265
39.6 to 49.5 GHz	0.0743	0.0290

Table 5.3: RMS and MV of PBFS method with α and k minimization

	RMS	MV
18.7 to 39.6 GHz	0.0931	-0.0204
18.7 to 49.5 GHz	0.1406	0.0713
39.6 to 49.5 GHz	0.0822	0.0327

For sake of completeness it is computed also the MV and the RMS of the error on a time series for the three scaling methods and for the three different scalings. This error is calculated as the difference between the real attenuation and the scaled one as reported in equation 5.8. Results are computed on the day of 26 May 1995 and they are reported in table 5.4

$$E_t = A_{REAL} - A_{SCALED} \tag{5.8}$$

Table 5.4: RMS and MV of the time series error

	Drufuca scaling		$PBFS$		$PBFS_{\alpha-k}$	
	MV	RMS	MV	RMS	MV	RMS
Error 18.7 to 39.6 GHz	0.0223	1.3154	-0.2322	1.2444	0.1150	1.7607
Error 18.7 to 49.5 GHz	0.2112	2.2517	-0.3760	1.9430	0.1920	2.8737
Error 39.6 to 49.5 GHz	0.2525	0.7873	-0.1399	0.4666	-0.0218	0.8242

The time series error for the time-span of one day (26 May 1995) for the $PBFS_{\alpha-k}$ scaling method from 39.6 to 49.5 GHz is reported in the figure 5.11

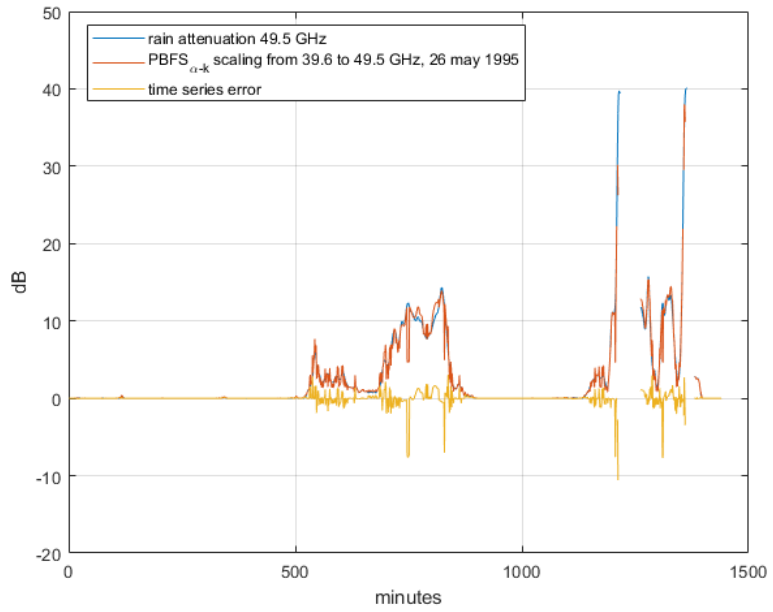

Figure 5.11: Time series error using $PBFS_{\alpha-k}$ scaling method from 39.6 to 49.5 GHz

6 | Conclusions and future developments

The aim of this work is to investigate the attenuations on the link between the satellite and the ground station for frequencies above 10 GHz and the pros and cons of the use of higher frequencies. It has been explained the frequency scaling and the reason to use it and a physically based frequency scaling (PBFS) model has been proposed. The PBFS has been compared with the well known Drufuca empirical scaling model. An optimization of the PBFS introducing a drop size distribution (DSD) model and obtaining α and k coefficients is performed. The scaling is done on rain attenuation retrieved from a biennial dataset (1995-1996) coming from the ground station of Spino D'Adda. The results of the two frequency scaling methods between rain attenuations in ccdf form has been evaluated with ITU-R P.311-18 error figure. The mean value (MV) and the root mean square (RMS) has been computed.

The RMS results obtained with the scaling from 18.7 to 39.6 GHz are 0.1646, 0.1552 and 0.0931 for Drufuca method, PBFS method and α and k optimization PBFS respectively. As it is possible to see the best results are coming from the last method. From the frequency of 18.7 to 49.5 GHz the RMS results are: 0.1936, 0.1874 and 0.1406. As it is possible to see the RMS is increasing when the frequency scaling has to cover a much higher leap. In the end the scaling is performed from 39.6 to 49.5 GHz and RMS results for three methods are: 0.1010, 0.0743 and 0.0822.

As it is possible to note from the RMS results the PBFS method and its optimization with the DSD model, guarantee a very good scaling maintaining the physics of the problem.

The possible future development are the use of a genetic algorithm to surpass the "brute force" approach applied in the PBFS method and get a local optimization for each point of the rain attenuation. Another future development it is to check how the methods behaves when they are used to scale in a greater frequency range.

Bibliography

[1] Allen, C. W. (1976), Astrophysical Quantities (Third ed.), Athlone Press, p. 119, ISBN 0-485-11150-0

[2] Rec. ITU-R P.676-13. "Attenuation by atmospheric gases". (2022)

[3] Enhancement of the Synthetic Storm Technique for the Prediction of Rain Attenuation Time Series at EHF Lorenzo Luini , Senior Member, IEEE, Alberto Panzeri, and Carlo G. Riva , Senior Member, IEEE.IEEE TRANSACTIONS ON ANTENNAS AND PROPAGATION, VOL. 68, NO. 7, JULY 2020

[4] A. Paraboni, M. D'Amico. "Radiopropagazione". (2002)

[5] Stefano Panzeri,Lorenzo Luini, 2018 FREQUENCY SCALING OF TROPOSPHERIC ATTENUATION FOR FUTURE SATCOM SYSTEMS OPERATING AT W BAND, Politecnico di Milano, Milano

[6] G. Drufuca, "Rain attenuation statistics for frequencies above 10GHz from rain gauge observations," Journal de Recherches Atmospheriques, vol. 8, p. 399, 1974.

[7] Lecture 34 Rayleigh Scattering, Mie Scattering. pag 339-348. Purdue University

[8] G. Mie, Beiträge zur Optik trüber Medien, speziell kolloidaler Metallösungen, Annalen der Physik, vol. 330, p. 377, 1908.

[9] Rec. ITU-R P.531-14. "Ionospheric propagation data and prediction methods required for the design of satellite networks and systems". (2019)

[10] Rec. ITU-R P.838-3. "Specific attenuation model for rain for use in prediction methods". (2005)

[11] Krebs, Gunter D. "Italsat 1, 2". Gunter's Space Page. Retrieved March 07, 2023, from `https://space.skyrocket.de/doc_sdat/italsat-1.htm`

[12] Summary of propagation results obtained in 5 years of ITALSAT experiment in Milano. Aldo Paraboni, Gino Masini, Mario Mauri, Roberto Polonio and Carlo Riva. INTERNATIONAL JOURNAL OF SATELLITE COMMUNICATIONS.Int. J. Satell. Commun. 17, 169-175 (1999).

[13] D.Hodge, Frequency scaling of rain attenuation, May 1977, pag 446 - 447, IEEE

[14] Recommendation ITU-R P.311-18, Acquisition, presentation and analysis of data in studies of radiowave propagation, 09/2021

[15] LI GUANJUN, An Analytical Model for the Attenuation and Phase Delay due to Rain in the 6-100 GHz Range, Politecnico di Milano, 2022

[16] `https://www.n2yo.com/satellite/?s=21055`

[17] Recommendation ITU-R P.453-11 (07/2015), The radio refractive index: its formula and refractivity data

[18] R.L. Olsen, D.V.Rogers, D.B.Hodge, "The aR^b relation in the calculation of rain attenuation" - IEEE Trans. Antennas Propagat. (1978)

[19] Kheirallah, H.; Olsen, R. Comparison of a one- and a two-frequency technique for frequency scaling of rain attenuation statistics.Electron. Lett. 1982, 18, 51

[20] Laster, J.D.; Stutzman, W.L. Frequency scaling of rain attenuation for satellite communication links. IEEE Trans. Antennas Propag.1995, 43, 1207–1216.

[21] Path Reduction Factor Modeling for Terrestrial Links Based on Rain Cell Growth P. O. Akuon and T. J. O. Afullo, Senior Member, SAIEE School of Electrical, Electronic and Computer Engineering, University of KwaZulu-Natal, Durban, 4041, South Africa. 13 - 15 September 2011

[22] Recommendation ITU-R P.840-8, Attenuation due to clouds and fog, 2019

A | Appendix A

Table A.1: oxygen coefficients ITU-676

f_0	a_1	a_2	a_3	a_4	a_5	a_6
50,474214	0,975000	9,651000	6,690000	0,000000	2,566000	6,850000
50,987745	2,529000	8,653000	7,170000	0,000000	2,246000	6,800000
51,503360	6,193000	7,709000	7,640000	0,000000	1,947000	6,729000
52,021429	14,320000	6,819000	8,110000	0,000000	1,667000	6,640000
52,542418	31,240000	5,983000	8,580000	0,000000	1,388000	6,526000
53,066934	64,290000	5,201000	9,060000	0,000000	1,349000	6,206000
53,595775	124,600000	4,474000	9,550000	0,000000	2,227000	5,085000
54,130025	227,300000	3,800000	9,960000	0,000000	3,170000	3,750000
54,671180	389,700000	3,182000	10,370000	0,000000	3,558000	2,654000
55,221384	627,100000	2,618000	10,890000	0,000000	2,560000	2,952000
55,783815	945,300000	2,109000	11,340000	0,000000	–1.172	6,135000
56,264774	543,400000	0,014000	17,030000	0,000000	3,525000	–0.978
56,363399	1331,800000	1,654000	11,890000	0,000000	–2.378	6,547000
56,968211	1746,600000	1,255000	12,230000	0,000000	–3.545	6,451000
57,612486	2120,100000	0,910000	12,620000	0,000000	–5.416	6,056000
58,323877	2363,700000	0,621000	12,950000	0,000000	–1.932	0,436000
58,446588	1442,100000	0,083000	14,910000	0,000000	6,768000	–1.273
59,164204	2379,900000	0,387000	13,530000	0,000000	–6.561	2,309000
59,590983	2090,700000	0,207000	14,080000	0,000000	6,957000	–0.776
60,306056	2103,400000	0,207000	14,150000	0,000000	–6.395	0,699000
60,434778	2438,000000	0,386000	13,390000	0,000000	6,342000	–2.825
61,150562	2479,500000	0,621000	12,920000	0,000000	1,014000	–0.584
61,800158	2275,900000	0,910000	12,630000	0,000000	5,014000	–6.619
62,411220	1915,400000	1,255000	12,170000	0,000000	3,029000	–6.759
62,486253	1503,000000	0,083000	15,130000	0,000000	–4.499	0,844000
62,997984	1490,200000	1,654000	11,740000	0,000000	1,856000	–6.675
63,568526	1078,000000	2,108000	11,340000	0,000000	0,658000	–6.139
64,127775	728,700000	2,617000	10,880000	0,000000	–3.036	–2.895

64,678910	461,300000	3,181000	10,380000	0,000000	–3.968	–2.590
65,224078	274,000000	3,800000	9,960000	0,000000	–3.528	–3.680
65,764779	153,000000	4,473000	9,550000	0,000000	–2.548	–5.002
66,302096	80,400000	5,200000	9,060000	0,000000	–1.660	–6.091
66,836834	39,800000	5,982000	8,580000	0,000000	–1.680	–6.393
67,369601	18,560000	6,818000	8,110000	0,000000	–1.956	–6.475
67,900868	8,172000	7,708000	7,640000	0,000000	–2.216	–6.545
68,431006	3,397000	8,652000	7,170000	0,000000	–2.492	–6.600
68,960312	1,334000	9,650000	6,690000	0,000000	–2.773	–6.650
118,750334	940,300000	0,010000	16,640000	0,000000	–0.439	0,079000
368,498246	67,400000	0,048000	16,400000	0,000000	0,000000	0,000000
424,763020	637,700000	0,044000	16,400000	0,000000	0,000000	0,000000
487,249273	237,400000	0,049000	16,000000	0,000000	0,000000	0,000000
715,392902	98,100000	0,145000	16,000000	0,000000	0,000000	0,000000
773,839490	572,300000	0,141000	16,200000	0,000000	0,000000	0,000000
834,145546	183,100000	0,145000	14,700000	0,000000	0,000000	0,000000

Table A.2: water vapour coefficients ITU-676

f_0	b_1	b_2	b_3	b_4	b_5	b_6
22,235080	0,107900	2,144000	26,380000	0,760000	5,087000	1,000000
67,803960	0,001100	8,732000	28,580000	0,690000	4,930000	0,820000
119,995940	0,000700	8,353000	29,480000	0,700000	4,780000	0,790000
183,310087	2,273000	0,668000	29,060000	0,770000	5,022000	0,850000
321,225630	0,047000	6,179000	24,040000	0,670000	4,398000	0,540000
325,152888	1,514000	1,541000	28,230000	0,640000	4,893000	0,740000
336,227764	0,001000	9,825000	26,930000	0,690000	4,740000	0,610000
380,197353	11,670000	1,048000	28,110000	0,540000	5,063000	0,890000
390,134508	0,004500	7,347000	21,520000	0,630000	4,810000	0,550000
437,346667	0,063200	5,048000	18,450000	0,600000	4,230000	0,480000
439,150807	0,909800	3,595000	20,070000	0,630000	4,483000	0,520000
443,018343	0,192000	5,048000	15,550000	0,600000	5,083000	0,500000
448,001085	10,410000	1,405000	25,640000	0,660000	5,028000	0,670000
470,888999	0,325400	3,597000	21,340000	0,660000	4,506000	0,650000
474,689092	1,260000	2,379000	23,200000	0,650000	4,804000	0,640000
488,490108	0,252900	2,852000	25,860000	0,690000	5,201000	0,720000
503,568532	0,037200	6,731000	16,120000	0,610000	3,980000	0,430000
504,482692	0,012400	6,731000	16,120000	0,610000	4,010000	0,450000
547,676440	0,978500	0,158000	26,000000	0,700000	4,500000	1,000000
552,020960	0,184000	0,158000	26,000000	0,700000	4,500000	1,000000
556,935985	497,000000	0,159000	30,860000	0,690000	4,552000	1,000000
620,700807	5,015000	2,391000	24,380000	0,710000	4,856000	0,680000
645,766085	0,006700	8,633000	18,000000	0,600000	4,000000	0,500000
658,005280	0,273200	7,816000	32,100000	0,690000	4,140000	1,000000
752,033113	243,400000	0,396000	30,860000	0,680000	4,352000	0,840000
841,051732	0,013400	8,177000	15,900000	0,330000	5,760000	0,450000
859,965698	0,132500	8,055000	30,600000	0,680000	4,090000	0,840000
899,303175	0,054700	7,914000	29,850000	0,680000	4,530000	0,900000
902,611085	0,038600	8,429000	28,650000	0,700000	5,100000	0,950000
906,205957	0,183600	5,110000	24,080000	0,700000	4,700000	0,530000
916,171582	8,400000	1,441000	26,730000	0,700000	5,150000	0,780000
923,112692	0,007900	10,293000	29,000000	0,700000	5,000000	0,800000
970,315022	9,009000	1,919000	25,500000	0,640000	4,940000	0,670000

987,926764	134,600000	0,257000	29,850000	0,680000	4,550000	0,900000
1780,000000	17506,000000	0,952000	196,300000	2,000000	24,150000	5,000000

Table A.3: rain coefficients ITU-838

$f[GHz]$	k_h	a_h	k_v	a_v
1,0000000	0,0000259	0,9691000	0,0000308	0,8592000
1,5000000	0,0000443	1,0185000	0,0000574	0,8957000
2,0000000	0,0000847	1,0664000	0,0000998	0,9490000
2,5000000	0,0001321	1,1209000	0,0001464	1,0085000
3,0000000	0,0001390	1,2322000	0,0001942	1,0688000
3,5000000	0,0001155	1,4189000	0,0002346	1,1387000
4,0000000	0,0001071	1,6009000	0,0002461	1,2476000
4,5000000	0,0001340	1,6948000	0,0002347	1,3987000
5,0000000	0,0002162	1,6969000	0,0002428	1,5317000
5,5000000	0,0003909	1,6499000	0,0003115	1,5882000
6,0000000	0,0007056	1,5900000	0,0004878	1,5728000
7,0000000	0,0019150	1,4810000	0,0014250	1,4745000
8,0000000	0,0041150	1,3905000	0,0034500	1,3797000
9,0000000	0,0075350	1,3155000	0,0066910	1,2895000
10,0000000	0,0121700	1,2571000	0,0112900	1,2156000
11,0000000	0,0177200	1,2140000	0,0173100	1,1617000
12,0000000	0,0238600	1,1825000	0,0245500	1,1216000
13,0000000	0,0304100	1,1586000	0,0326600	1,0901000
14,0000000	0,0373800	1,1396000	0,0412600	1,0646000
15,0000000	0,0448100	1,1233000	0,0500800	1,0440000
16,0000000	0,0528200	1,1086000	0,0589900	1,0273000
17,0000000	0,0614600	1,0949000	0,0679700	1,0137000
18,0000000	0,0707800	1,0818000	0,0770800	1,0025000
19,0000000	0,0808400	1,0691000	0,0864200	0,9930000
20,0000000	0,0916400	1,0568000	0,0961100	0,9847000
21,0000000	0,1032000	1,0447000	0,1063000	0,9771000
22,0000000	0,1155000	1,0329000	0,1170000	0,9700000
23,0000000	0,1286000	1,0214000	0,1284000	0,9630000
24,0000000	0,1425000	1,0101000	0,1404000	0,9561000
25,0000000	0,1571000	0,9991000	0,1533000	0,9491000
26,0000000	0,1724000	0,9884000	0,1669000	0,9421000
27,0000000	0,1884000	0,9780000	0,1813000	0,9349000
28,0000000	0,2051000	0,9679000	0,1964000	0,9277000

29,0000000	0,2224000	0,9580000	0,2124000	0,9203000
30,0000000	0,2403000	0,9485000	0,2291000	0,9129000
31,0000000	0,2588000	0,9392000	0,2465000	0,9055000
32,0000000	0,2778000	0,9302000	0,2646000	0,8981000
33,0000000	0,2972000	0,9214000	0,2833000	0,8907000
34,0000000	0,3171000	0,9129000	0,3026000	0,8834000
35,0000000	0,3374000	0,9047000	0,3224000	0,8761000
36,0000000	0,3580000	0,8967000	0,3427000	0,8690000
37,0000000	0,3789000	0,8890000	0,3633000	0,8621000
38,0000000	0,4001000	0,8816000	0,3844000	0,8552000
39,0000000	0,4215000	0,8743000	0,4058000	0,8486000
40,0000000	0,4431000	0,8673000	0,4274000	0,8421000
41,0000000	0,4647000	0,8605000	0,4492000	0,8357000
42,0000000	0,4865000	0,8539000	0,4712000	0,8296000
43,0000000	0,5084000	0,8476000	0,4932000	0,8236000
44,0000000	0,5302000	0,8414000	0,5153000	0,8179000
45,0000000	0,5521000	0,8355000	0,5375000	0,8123000
46,0000000	0,5738000	0,8297000	0,5596000	0,8069000
47,0000000	0,5956000	0,8241000	0,5817000	0,8017000
48,0000000	0,6172000	0,8187000	0,6037000	0,7967000
49,0000000	0,6386000	0,8134000	0,6255000	0,7918000
50,0000000	0,6600000	0,8084000	0,6472000	0,7871000
51,0000000	0,6811000	0,8034000	0,6687000	0,7826000
52,0000000	0,7020000	0,7987000	0,6901000	0,7783000
53,0000000	0,7228000	0,7941000	0,7112000	0,7741000
54,0000000	0,7433000	0,7896000	0,7321000	0,7700000
55,0000000	0,7635000	0,7853000	0,7527000	0,7661000
56,0000000	0,7835000	0,7811000	0,7730000	0,7623000
57,0000000	0,8032000	0,7771000	0,7931000	0,7587000
58,0000000	0,8226000	0,7731000	0,8129000	0,7552000
59,0000000	0,8418000	0,7693000	0,8324000	0,7518000
60,0000000	0,8606000	0,7656000	0,8515000	0,7486000
61,0000000	0,8791000	0,7621000	0,8704000	0,7454000
62,0000000	0,8974000	0,7586000	0,8889000	0,7424000
63,0000000	0,9153000	0,7552000	0,9071000	0,7395000

64,0000000	0,9328000	0,7520000	0,9250000	0,7366000
65,0000000	0,9501000	0,7488000	0,9425000	0,7339000
66,0000000	0,9670000	0,7458000	0,9598000	0,7313000
67,0000000	0,9836000	0,7428000	0,9767000	0,7287000
68,0000000	0,9999000	0,7400000	0,9932000	0,7262000
69,0000000	1,0159000	0,7372000	1,0094000	0,7238000
70,0000000	1,0315000	0,7345000	1,0253000	0,7215000
71,0000000	1,0468000	0,7318000	1,0409000	0,7193000
72,0000000	1,0618000	0,7293000	1,0561000	0,7171000
73,0000000	1,0764000	0,7268000	1,0711000	0,7150000
74,0000000	1,0908000	0,7244000	1,0857000	0,7130000
75,0000000	1,1048000	0,7221000	1,1000000	0,7110000
76,0000000	1,1185000	0,7199000	1,1139000	0,7091000
77,0000000	1,1320000	0,7177000	1,1276000	0,7073000
78,0000000	1,1451000	0,7156000	1,1410000	0,7055000
79,0000000	1,1579000	0,7135000	1,1541000	0,7038000
80,0000000	1,1704000	0,7115000	1,1668000	0,7021000
81,0000000	1,1827000	0,7096000	1,1793000	0,7004000
82,0000000	1,1946000	0,7077000	1,1915000	0,6988000
83,0000000	1,2063000	0,7058000	1,2034000	0,6973000
84,0000000	1,2177000	0,7040000	1,2151000	0,6958000
85,0000000	1,2289000	0,7023000	1,2265000	0,6943000
86,0000000	1,2398000	0,7006000	1,2376000	0,6929000
87,0000000	1,2504000	0,6990000	1,2484000	0,6915000
88,0000000	1,2607000	0,6974000	1,2590000	0,6902000
89,0000000	1,2708000	0,6959000	1,2694000	0,6889000
90,0000000	1,2807000	0,6944000	1,2795000	0,6876000
91,0000000	1,2903000	0,6929000	1,2893000	0,6864000
92,0000000	1,2997000	0,6915000	1,2989000	0,6852000
93,0000000	1,3089000	0,6901000	1,3083000	0,6840000
94,0000000	1,3179000	0,6888000	1,3175000	0,6828000
95,0000000	1,3266000	0,6875000	1,3265000	0,6817000
96,0000000	1,3351000	0,6862000	1,3352000	0,6806000
97,0000000	1,3434000	0,6850000	1,3437000	0,6796000
98,0000000	1,3515000	0,6838000	1,3520000	0,6785000

99,0000000	1,3594000	0,6826000	1,3601000	0,6775000
100,0000000	1,3671000	0,6815000	1,3680000	0,6765000
120,0000000	1,4866000	0,6640000	1,4911000	0,6609000
150,0000000	1,5823000	0,6494000	1,5896000	0,6466000
200,0000000	1,6378000	0,6382000	1,6443000	0,6343000
300,0000000	1,6286000	0,6296000	1,6286000	0,6262000
400,0000000	1,5860000	0,6262000	1,5820000	0,6256000
500,0000000	1,5418000	0,6253000	1,5366000	0,6272000
600,0000000	1,5013000	0,6262000	1,4967000	0,6293000
700,0000000	1,4654000	0,6284000	1,4622000	0,6315000
800,0000000	1,4335000	0,6315000	1,4321000	0,6334000
900,0000000	1,4050000	0,6353000	1,4056000	0,6351000
1000,0000000	1,3795000	0,6396000	1,3822000	0,6365000

TLEs of ITALSAT-1 [16]:

1 21055U 91003A 23074.79702340 -.00000205 00000-0 00000-0 0 9992

2 21055 14.8229 0.6151 0015543 31.8520 160.4573 0.99955320105195

B | Appendix B

In appendix B the function used to perform frequency scaling is reported:

```
function [STIMA,best_R,best_prf,E]=minimizzami(A_real,k,a,i,j
    )

% The function obtain the best R and PRF minimizing the
    difference between
% A_real and A_down. This function is used in a frequency
    scaling approach.
% input:
%  -A_down: attenuation at lower frequency
%  -A_real: attenuation at goal frequency
%  -k and a: coefficient of A=k*R^a*prf*A_down, obtained from
     ITU 838 model
%  -i and j: length of R and prf vector, determine the
    precision of this
%            function, be careful a value too high will give
    a run-out memory
%            error or a very high computation time,
%            a good solution is to use i=25, j=15 but can be
    changed depending on
%            situation. Another possibility (not implemented)
     is to have a logarithmic
%            distribution for R.
% output:
%  -STIMA: estimated attenuation vector
%  -best_R: vector of best rain rate
%  -best_prf: vector of best path reduction factor
%  -E: error vector between real and estimated attenuation
%
% VERSION: 1.0, 1/03/2023, Davide Allievi
```

```
clear STIMA best_R best_prf E E_new best_R_position
   best_prf_position R prf

R=linspace(0.1,200,i);
prf=linspace(0.1,10,j);

confronto=zeros(i,j);
for m=1:length(R)
    for b=1:length(prf)
        confronto(m,b)=k*R(m)^a*prf(b);
    end
end

L=length(A_real);

UNO=ones(length(R),length(prf));
treD=ones(1,L);

for m=1:length(R)
    for b=1:length(prf)
        for n=1:L
%         confronto(m,b,n)=confronto(m,b)*A_down(n);
        confronto(m,b,n)=confronto(m,b)*treD(n);
        AA(m,b,n)=UNO(m,b)*A_real(n);
        end
    end
end

E=abs(confronto-AA);

E_new=zeros(1,length(A_real));best_R_position=E_new;
   best_prf_position=E_new;best_R=E_new;best_prf=E_new;STIMA=
   E_new;
for m=1:L
    if isnan(A_real(m))
        best_R(m)=NaN;
        best_prf(m)=NaN;
```

```
        STIMA(m)=NaN;
    else
        E_new(m)=min(min(E(:,:,m)));
    if isnan(E_new(m))
        best_R(m)=NaN;
        best_prf(m)=NaN;
        STIMA(m)=NaN;
%         E_new(m)=min(min(E(:,:,m),[],'omitnan'),[],'omitnan
   ');
    else
        [best_R_position(m),best_prf_position(m)]=find(E(:,:,
           m)==E_new(m));
        best_R(m)=R(best_R_position(m));
        best_prf(m)=prf(best_prf_position(m));
        STIMA(m)=k.*best_R(m).^a.*best_prf(m);
    end
    end

end

% from 18.7 GHz to 39.6 GHz
A39R_second=kappa39_itu.*best_R18.^alfa39_itu.*A_R_18.*
   best_prf18./(kappa18_itu.*best_R18.^alfa18_itu.*best_prf18
   );
% from 18.7 GHz to 49.5 GHz
A49R_second=kappa49_itu.*best_R18.^alfa49_itu.*A_R_18.*
   best_prf18./(kappa18_itu.*best_R18.^alfa18_itu.*best_prf18
   );
% from 39.6 GHz to 49.5 GHz
A49R_second_39to49=kappa49_itu.*best_R39.^alfa49_itu.*A_R_39
   ./(kappa39_itu.*best_R39.^alfa39_itu);
```

List of Figures

List of Tables

Acknowledgements

Ringrazio il mio relatore Lorenzo Luini che mi ha seguito durante l'esperienza di tesi rendendosi sempre disponibile per chiarimenti e delucidazioni.
Ringrazio la mia fidanzata Camilla che mi è stata sempre vicino.
Ringrazio i miei genitori per avermi spinto sempre a continuare.